1-1-1993

Kerr effect and wide angle light scattering studies of a para-aromatic polyamide in dilute solution/

Aniruddha J. Shere
University of Massachusetts Amherst

KERR EFFECT AND WIDE ANGLE LIGHT SCATTERING STUDIES OF A PARA-AROMATIC POLYAMIDE IN DILUTE SOLUTION

A Dissertation Presented

by

ANIRUDDHA J. SHERE

Submitted to the Graduate School of the
University of Massachusetts in partial fulfillment
of the requirements for the degree of

DOCTOR OF PHILOSOPHY

February 1993

Department of Polymer Science and Engineering

KERR EFFECT AND WIDE ANGLE LIGHT SCATTERING STUDIES OF A PARA-AROMATIC POLYAMIDE IN DILUTE SOLUTION

A Dissertation Presented

by

ANIRUDDHA J. SHERE

Approved as to style and content by:

Richard S. Stein, Co-chair

Murugappan Muthukumar, Co-chair

David A. Hoagland, Member

Scott W. Barton, Member

William J. MacKnight, Head
Polymer Science and Engineering

Dedicated

to my Parents

ACKNOWLEDGEMENTS

It is a great pleasure to express my deepest thanks and gratitude to my advisors Professor Richard S. Stein and Professor Murugappan Muthukumar for their guidance throughout the course of this work. I would also like to thank my dissertation committee members, Professor Scott Barton and Professor David Hoagland for their suggestions and encouragement.

Special thanks to Dr. Ravi Saraf of IBM, T. J. Watson Research Center, Yorktown Heights, New York for giving me the opportunity to work at the Watson Research Center, and providing help in setting up the Kerr effect apparatus. His unflagging energy, and the shear joy he derives from his work has been inspirational.

I would like to extend my thanks to Dr. Russell Gaudiana, Dr. Norman Weeks, Dr. Vivek Soni, Dr. Parag Mehta and Dr. Saroj Roy for providing the polyamide samples and helping with the light scattering and viscometry measurements. I would also like to thank Professor Langley and Professor Hoagland for allowing access to their wide angle light scattering instruments.

It gives me great pleasure to acknowledge the help and dear friendship of my colleague Murali Sethumadhavan who assisted in the dilute solution characterization of the

polyamide samples. I would also like to thank all my friends who made the time spent at Amherst so enjoyable.

Finally and above all, I would like to thank my parents whose never wavering support and encouragement helped me beyond measure in completing this dissertation.

ABSTRACT

KERR EFFECT AND WIDE ANGLE LIGHT SCATTERING STUDIES OF A PARA-AROMATIC POLYAMIDE IN DILUTE SOLUTION

FEBRUARY 1993

ANIRUDDHA J. SHERE, B.S., INDIAN INSTITUTE OF TECHNOLOGY

M.S., UNIVERSITY OF AKRON

Ph.D., UNIVERSITY OF MASSACHUSETTS

Directed by: Professor Richard S. Stein

A series of para-linked aromatic polyamides synthesized with the aim of making optically uniaxial, transparent films and fibers for optical applications, are found to have anomalous properties. Stretched films of these polyamides are highly birefringent and non-crystalline at the same time. These rod-like polyamides do not form lyotropic solutions and are soluble in common solvents like THF, unlike other rod-like polymers. With the goal of understanding this behavior from a molecular standpoint we have quantitatively characterized the geometric, optical and hydrodynamic properties of one of these polyamides.

Wide angle light scattering measurements on polyamide in THF were used in conjunction with electric birefringence measurements to determine the weight average molecular weight, M_w, the root mean square z-averaged radius of gyration, R_{gz}, the apparent second virial coefficient, A_{2app} and the monomer molecular anisotropy ratio ε. The

polydispersity correction was applied theoretically by assuming the most probable distribution. Hydrodynamic and optical properties were determined with viscometry and differential refractometry respectively.

The aromatic polyamide studied can be satisfactorily modeled as a Kratky-Porod wormlike chain with a persistence length of 220±50 Å and a monomer optical anisotropy ratio of 2.3±0.3. The excluded volume effect is found to be negligible in THF at 25 °C.

The small axial ratio of 35 may be partly responsible for the non-lyotropic behavior. The refractive index of 1.67 is in good agreement with that of similar polyamides. The repeat unit has a high optical anisotropy leading to highly birefringent films. It is also conclusively established that there is no aggregation due to H-bonding in the absence of moisture.

The light scattering theory of Nagai and the hydrodynamic theory adopted for semiflexible chains is found to hold very well for the polyamide studied. Based on the agreement between experiment and theory we infer that the molecular weight distribution is of the most probable type. Our depolarized light scattering data indicate that the straight line behavior observed in Zimm plots even for $R_g^2q^2 > 1$, upto $R_g^2q^2$ of 3.5 is due to the combined effect of polydispersity, large size and optical anisotropy of the molecule.

TABLE OF CONTENTS

LIST OF TABLES

LIST OF FIGURES

CHAPTER 1

INTRODUCTION

Kerr Effect

Electric birefringence has been extensively used for characterizing optical properties of polymers and small molecules[1,2,3,4]. The optical anisotropy obtained from Kerr effect experiments can used in conjunction with wide angle light scattering data to determine the equilibrium rigidity of a polymer chain[5,6]. The chain rigidity can be characterized by Kuhn step length or persistence length. Moreover, Kerr effect couples strongly to molecular aggregation due to the sensitivity of optical anisotropy to the geometric arrangement of Kuhn segments[6,7,8]. These considerations have motivated the molecular conformational study of a 2,2'-disubstituted biphenyl polyamide and poly(di-n-hexyl silane) using Kerr effect, light scattering and other dilute solution techniques. The chemical structure of these two polymers are shown in Figure 1 and Figure 2 respectively.

Polyamide

Several processable and highly oriented polyamides have been synthesized over the last decade[9,10,11]. A series of para-linked aromatic polyamides have been designed and synthesized by Roger and et al.[12,13] with the aim of making

highly oriented, optically uniaxial, colorless, transparent films and fibers suitable for optical applications. Although most of these goals were met, obtaining oriented films by casting or extrusion from polymer solutions was found to be difficult since none of these rod=like polyamides formed lyotropic solutions. Stretched films of these polyamides are highly birefringent ($\Delta n = 0.7$) and noncrystalline ($X_c = 5\%$) at the same time. Unlike other rod-like polymers like Kevlar, PBT, PPTA etc these polyamides are soluble in common solvents like THF and acetone.

The goal of our investigation is to understand this anomalous behavior from a molecular standpoint. To this end we have quantitatively characterized the geometric, optical, electrical and hydrodynamic properties of the polyamide shown in Figure 1. Wide angle light scattering measurements were used in conjunction with electric birefringence measurements to determine the weight average molecular weight, M_w, the root mean square z-averaged radius of gyration, R_{Gz}, the apparent second virial coefficient, A_{2app}, and the monomer anisotropy ratio ε. Measurements were carried out in tetrahydrofuran as a solvent for the polyamide. Polydispersity corrections were applied theoretically by assuming the most probable distribution. Depolarized light scattering was performed to check the monomer anisotropy ratio obtained from wide angle light scattering. Hydrodynamic properties were determined in THF with

viscometry. Differential refractometry was used to determine optical properties of the polyamide.

Poly(di-n-hexyl silane)

Poly(di-n-hexyl silane) is one of the many substituted organosilane polymers which have recently been synthesized that are soluble in common organic solvents[14]. These polymers are of technological interest as ceramic precursors[15], lithograhic materials, and prospective non-linear optical materials. The electronic spectra of polysilane derivatives are very unusual in that they absorb strongly in the UV in spite of the fact that the backbone is comprised solely of saturated σ links. This is due to $\sigma-\sigma^*$ or a σ - Si^{3d} transition[16]. Since there is considerable σ delocalization in the backbone, electron absorption has been suggested to be dependent on the backbone conformation.

Aliphatically substituted polydiorgano-silylenes display reversible thermochromic behavior in solution with a bathochromic shift occurring with decreasing temperature[17,18]. This low temperature transition at -25 °C is argued to be due to a continuously increasing relative population of trans conformation in the polymer backbone with cooling. This suggests investigation of the chain conformation at low temperatures. Several explanations have been proposed for this transition[17]. Static light scattering studies[19] on a very high molecular weight (M_w = 6 x 10^6)

sample of poly(di-n-hexyl silane) in hexane show a large increase in the depolarized scattering. This indicates the formation of an extended conformation. These studies were carried out at a very low concentration (c = 0.017 gm/lit) to prevent precipitation at low temperature. Additional evidence for coil to rod transition is the scattering fluctuations observed[18] due to incipient gelation following rod formation.

Our goal is to investigate the molecular conformation at low temperature using small angle X-ray scattering, small angle neutron scattering and electric birefringence measurement. SAXS and SANS experiments were performed on poly(di-n-hexyl silane) solutions in hexane to measure the persistence length. Kerr effect experiments were performed to determine the optical anisotropy of the polymer at low temperatures.

Models

Freely Rotating Chain Model

The freely rotating chain[20] is often used to model flexible polymers. In this model the chain has free rotation about each of the N bonds with length *l* and valence angle ψ. Let

$$C = \cos(\pi-\psi) \qquad (1.1)$$

$$\gamma = \frac{3C^2 - 1}{2} \qquad (1.2)$$

Let us first define the optical anisotropy of a polymer segment, ζ_o, in terms of the principal polarizabilities α_1, α_2 and α_3 of the segment[21,22]

$$\zeta_o^2 = \frac{(\alpha_1-\alpha_2)^2 + (\alpha_1-\alpha_3)^2 + (\alpha_2-\alpha_3)^2}{2(\alpha_1+\alpha_2+\alpha_3)^2} \qquad (1.3)$$

For the case of segments with cylindrical symmetry $\alpha_2 = \alpha_3$ and α_1, this reduces to

$$\zeta_o = \frac{\alpha_1 - \alpha_2}{\alpha_1 + 2\alpha_2} \qquad (1.4)$$

In this case, ζ_o lies in the range $-1/2 < \zeta_o < 1$. The overall anisotropy, ζ, for a polymer chain can be defined as an average of ζ_o for each chain segment over conformation space. Also, the radius of gyration, R_g, is defined by

$$R_g^2 = \frac{1}{N} \sum_{j=1}^{N} r_j^2$$

where r_j is the distance of segment j from the center of mass of the molecule.

The chain anisotropy, ζ, has been calculated for the freely rotating chain[23],

$$\zeta^2 = \frac{\zeta_o^2}{N}\left\{\frac{1+\gamma}{1-\gamma} - \frac{2\gamma\ 1-\gamma^N}{N(1-\gamma)^2}\right\} \qquad (1.5)$$

where γ is given by equation (1.2) and $\gamma \neq 1$. In fact $\gamma = 1$ is the trivial case of a polymer chain with bond angle of 180° forming a rod. The mean square radius gyration, R_g^2, has also been calculated for this model[24],

$$R_g^2 = \frac{N\ l^2}{6}\frac{1 + C}{1 - C} \qquad (1.6)$$

for large N. Here c is given by equation (1.1).

In the case of large N and α = 90°, the square of the radius of gyration for such a chain is given by $R_g^2 = Nl^2/6$. One can use a statistical model to simulate the chain[25], with an equivalent segment length or Kuhn statistical segment length b defined so that $R_g^2 = n_k b^2/6$ and the contour length $L = n_k b$. The molecular weight exponent of 0.5 for R_g is a characteristic of a random walk.

$$R_g \sim M^{0.5}$$

This is the condition for a flexible chain[26]. Very short or stiff chains do not meet this criteria since there are an insufficient number of statistically independent segments. The limiting geometry here is a rigid rod which has a single segment. A model which encompasses both the limits of rod and random coil is the wormlike chain.

Persistent Chain Model

Consider a model chain with N bonds of length *l* joined with bond angle ψ, where free rotation about bonds is allowed. ψ and *l* do not necessarily represent true bond angle and bond length respectively. Suppose that the first bond $\mathbf{r}_1$ is placed in the direction of the positive z axis as shown in Figure 3. For large N, the average z-component of the end-to-end vector **R** is given by[26],

$$\lim_{N\to\infty} \langle \mathbf{R}.\mathbf{e}_z \rangle = \frac{l}{1 + \mathrm{Cos}(\psi)} = a \qquad (1.7)$$

The length a is referred to as the persistence length of the chain.

A wormlike chain is the limiting continuous chain obtained from the above discrete chain by letting *l*-->0 and ψ -->π under the condition that $l/(1 + \mathrm{Cos}(\psi)) = a$ and $Nl = L$ remains constant. For such a chain the radius of gyration is given by[26],

$$R_g^2 = \frac{a^2}{3} \times g_1 \qquad (1.8)$$

where

$$g_1 = 1 - \frac{3}{x} + \frac{6}{x^2} - \frac{6}{x^3} + \frac{6}{x^3} e^{-x} \qquad (1.9)$$

$$x = \frac{L}{a} \qquad (1.10)$$

L is contour length of the polymer chain.

Molecular chain anisotropy, δ, is defined by

$$\zeta^2 = \frac{(\alpha_{||} - \alpha_{\perp})^2}{(\alpha_{||} + 2\alpha_{\perp})^2} \qquad (1.11)$$

where $\alpha_{||}$ and $\alpha_{\perp}$ are optical polarizabilities of the polymer chain, parallel and perpendicular to the end-to-end vector respectively. For a worm-like chain[27]

$$\zeta^2 = \frac{2}{27} \varepsilon^2 \frac{g_2}{x} \qquad (1.12)$$

where

$$g_2 = 1 - \frac{1}{3x} + \frac{1}{3x} e^{-3x} \qquad (1.13)$$

$$\varepsilon = \frac{3(\alpha_1 - \alpha_2)}{(\alpha_1 + 2\alpha_2)} \qquad (1.14)$$

α_1 and α_2 are optical polarizabilities parallel and perpendicular to the monomer as indicated in Figure 1. It is worthwhile to note that $\varepsilon = 3$ for a rod-like monomer with $\alpha_1 >>> \alpha_2$, and $\varepsilon = -3/2$ for a disc-like monomer with $\alpha_2 >>> \alpha_1$.

For the polyamide molecule studied, bond angles θ_1 and θ_2 shown in Figure 4 are not equal, but differ by $\Delta\theta$[28,29]. This causes an angular bending of the chain axis by $\Delta\theta$ (about 10°)

with each monomer step, which leads to wormlike behavior. Next we consider the asymptotic limits of a wormlike chain:

Case 1 $x \ll 1$ is the Rod limit.

$$R_g^2 = \frac{L^2}{12} \tag{1.15}$$

$$\zeta^2 = \frac{\varepsilon^2}{9} \tag{1.16}$$

Case 2 $x \to \infty$ is the Gaussian coil limit.

$$R_g^2 = \frac{n_k\, b^2}{6} \tag{1.17}$$

$$\zeta^2 = \frac{\varepsilon^2}{9n_k} \tag{1.18}$$

where the chain is assumed to consist of n_k Kuhn steps of length b such that $n_k b = L$ and $b = 2a$.

Case 3 Intermediate values of x correspond to a semiflexible chain.

Polydispersity Effect

The polyamide samples were synthesized by a polycondensation reaction between a diamine and a diacid chloride. Hence, the samples are polydisperse with molecular weight distribution approximated by the most probable distribution. Attempts to determine the molecular weight

distribution using gel permeation chromatography by the polymer research group at the Polaroid Corporation, for similar polyamides have failed due to the specific interaction of the polyamide to the column material. Due to the lack of a better alternative we have assumed the most probable distribution[30,31], f(n),

$$f(n) = y^2 \, n \, e^{-yn} \qquad (1.19)$$

where $y = \frac{2}{n_w}$

n is the degree of polymerization and n_w is the weight average degree of polymerization. The validity of this assumption will be tested by experimental data. The theoretical molecular weight distribution shown in Figure 5 for various degrees of conversion indicates that the molecular weight distribution is a strong function of the degree of conversion. Hence, it is very important to apply the polydispersity correction to static light scattering, Kerr effect and viscometry measurements.

CHAPTER 2

THEORY

Kerr Effect

When a fluid is subjected to an uniform electric field, polar or optically anisotropic molecules get partially oriented with respect to the electric field. In the case of optically asymmetric molecules, the fluid becomes optically anisotropic. This effect is called electric birefringence, or the Kerr electro-optic effect[32]. The phenomenon was initially studied in solids and liquids[33]. It also occurs in gases, but to a lower extent due to the lower density. Polymer molecules in solution exhibit a large Kerr effect because the orientation of a molecule in an electric field depends upon its size as well as electric asymmetry.

The theory of Kerr effect in gases has been relatively well understood. Hence Kerr effect has been used to study molecular structure of gases[33]. It has also been investigated in solutions of organic molecules, and in polymer solution.

The Kerr cell arrangement shown in Figure 6 illustrates the phenomenological aspects of the Kerr effect. A linearly polarized light beam is incident on a medium which is placed between two plane parallel electrodes connected to an external voltage source. The direction of polarization of

the light beam is usually oriented 45° with respect to the direction of the applied field. The electric vector of the incident light, E, may be decomposed into two components, one parallel to the direction of the applied electric field, E_{11}, and the other perpendicular to the direction of the applied field, $E_{\perp}$. These two vectors are in phase as the light enters the medium. Due to the influence of the external electric field the medium will have different refractive indices in the parallel and the perpendicular directions. Therefore, the two component waves travel through the medium at different velocities, and in general, emerge out of phase. The resultant vector, E_o, of the addition of these two component waves is a vector which, in general, is not in the plane of polarization of the incident wave. Thus the light leaving the Kerr cell is elliptically polarized. When the external electric field is absent, the light coming out of the Kerr cell is plane polarized, and hence can be extinguished by means of a crossed polarizer. In the presence of the electric field the emergent light has, in general, a component perpendicular to the incident polarized light vector. Thus a portion of the light is transmitted by the analyzer. The intensity of transmitted light relative to that of the incident light, is directly related to the optical retardation produced by the applied electric field.

For the parallel light component, the optical path length of the cell may be expressed by equation (2.1a).

$$N_{||} = \frac{L\, n_{||}}{\lambda_o} \qquad (2.1a)$$

where $N_{||}$ is the number of wavelengths of light in the cell of length L, $n_{||}$ is the refractive index for the parallel light component, and λ_o is the wavelength of the light in vacuum. Similarly, equation (2.1b) gives the number of wavelengths of light in the cell of length L for the perpendicular component

$$N_{\perp} = \frac{L\, n_{\perp}}{\lambda_o} \qquad (2.1b)$$

Hence the optical path difference in radians, δ, is given by

$$\delta = 2\pi(N_{||} - N_{\perp}) = \frac{2\pi L\, \Delta n}{\lambda_o} \qquad (2.2)$$

where $\Delta n = n_{||} - n_{\perp}$, is the birefringence of the medium. The value of retardance δ can be obtained from measurements of the increase in the intensity of the light produced by application of the electric field to the medium between crossed polarizer and analyzer at 45°.

In 1875 Kerr[32] observed that at low electric field strengths the birefringence at a given wavelength is proportional to the square of the electric field. This is called as the Kerr law, which holds for most substances and is given by

$$\Delta n = n_{||} - n_{\perp} = B\, \lambda\, E^2 \qquad (2.3)$$

where E is the electric field strength, B is the Kerr constant and λ is the wavelength of the light in the medium. The units of B and E are cm/SV^2 and SV/cm respectively.

The Kerr constant, B, can be positive or negative as shown in Figure 7. For example for $ClCH_2CH_2Cl$ the axis of maximum polarizability is coincident with the direction of the permanent dipole moment, and since molecular orientation is mainly caused by the permanent dipole aligning with the field, $n_{||}$ is greater than $n_{\perp}$. In the case of diethylether and tetrahydrofuran the Kerr constant is negative because direction of maximum polarizability is perpendicular to the permanent dipole moment.

We now define "molecular and specific Kerr constant", ${}_mK$ and ${}_sK$, since these quantities can be conveniently calculated from observations on solutions. The molecular Kerr constant is[2]

$$ {}_mK = \frac{6n_1 \lambda B_1 M_1}{(n_1^2+2)^2 (\varepsilon_1+2)^2 d_1} \qquad (2.4) $$

where M_1 is the molecular weight, n_1 the refractive index, ε_1 the dielectric constant, and d_1 the density of the medium under examination, while λ is the wavelength of the light used to determine B_1. The specific Kerr constant is related to B_1 by

$$ {}_sK = \frac{6n_1 \lambda B_1}{(n_1^2+2)^2 (\varepsilon_1+2)^2 d_1} \qquad (2.5) $$

The specific Kerr constant, ${}_sK$, quantifies the birefringence due to unit mass of the substance and unit electric field strength. Similarly the molecular Kerr constant represents birefringence due to an unit mole of the substance and an unit electric field.

Next, we describe the procedure of obtaining Kerr constant of a solute as developed by Le Fevre[2]. To compute the molar Kerr constant of a solute the measurement of four physical properties of a solution of known concentration is required. Solvents which have small electric birefringence are used to make the solutions. Usually nonpolar solvents like carbon tetrachloride, benzene, hexane, cyclohexane or dioxane are recommended in the order of preference. A series of solutions of increasing concentrations are made, and the weight fraction of solute, w_2, of each calculated. For each solution the following physical quantities are determined : (1) the Kerr constant B; (2) the dielectric constant ε; (3) the density d; (4) the refractive index n (at the same wavelength at which B is measured). For a strongly polar substance one would expect a very large Kerr effect, hence it is preferable to keep the solutions dilute. For nonpolar substances it is helpful to use solutions up to solute weight

fraction of 0.05. LeFevre and LeFevre[34] have derived the expression (2.6) for the specific Kerr constant of a solute at infinite dilution.

$$ {}_sK_2 = {}_sK_1 \ (1-a_2+a_3+a_4-Ha_3-Ja_1\varepsilon_1) \qquad (2.6) $$

where

$$ H = \frac{4n_1^2}{n_1^2+2} $$

$$ J = \frac{2}{\varepsilon_1+2} $$

H, J and ${}_sK_1$ are constants for a given solvent at a specified temperature. The value of a_1, a_2, a_3 and a_4 are obtained by assuming that the dielectric constants, densities, refractive indices, and Kerr constants of the solutions depend on the concentrations in a linear manner in the limit of small concentration.

$$ \varepsilon = \varepsilon_1 \ (1 + a_1 w_2) \qquad (2.7) $$

$$ d = d_1 \ (1 + a_2 w_2) \qquad (2.8) $$

$$ n = n_1 \ (1 + a_3 w_2) \qquad (2.9) $$

$$ B = B_1 \ (1 + a_4 w_2 + a_5 w_2^2) \qquad (2.10) $$

If B shows a curvature when plotted against w_2, the change in Kerr constant in passing from solvent to solution (ΔB) is fitted to a power series in w_2.

Polydispersity Effect

Consider a binary solution of a solute(2) and solvent(1). We assume that the solution is dilute so that the birefringence is additive and the total birefringence of the solution is given by

$$\Delta n_{total} = \Delta n_1 + \Delta n_2 \qquad (2.11)$$

where Δn_1 and Δn_2 are the electric birefringences due to solvent and solute. Rewriting equation (2.11) in terms of Kerr law we get

$$B_{12}\lambda E^2 = B_1\lambda E^2 + B_2\lambda E^2$$

where B_{12} is the effective Kerr constant of the polymer-solvent mixture. Hence,

$$B_{12} = B_1 + B_2 \qquad (2.12)$$

Rearranging the expression using the specific Kerr constant, ${}_sK_2$ as given by equation (2.5) we have

$$B_{12} = \frac{(n^2+2)^2\ (\varepsilon+2)^2}{6n\lambda}\ {}_sK_{12}\ \frac{(m_1+m_2)}{V} \qquad (2.13)$$

where m_1 and m_2 are masses of solvent and solute in volume V, the solution volume traversed by the light beam, respectively. Also, n is the refractive index and ε is the dielectric constant of the solution. B_1 and B_2 can be obtained from ${}_sK_1$ and ${}_sK_2$ by considering internal field effect due the surrounding solution.

$$B_1 = \frac{(n^2+2)^2\ (\varepsilon+2)^2}{6n\lambda}\ {}_sK_1\ \frac{m_1}{V} \qquad (2.14)$$

$$B_2 = \frac{(n^2+2)^2\ (\varepsilon+2)^2}{6n\lambda}\ {}_sK_2\ \frac{m_2}{V} \qquad (2.15)$$

Substituting equation (2.13), (2.14) and (2.15) in equation (2.12), and rearranging we have

$${}_sK_{12} = {}_sK_1\ w_1 + {}_sK_2\ w_2 \qquad (2.16)$$

where w_1 and w_2 are weight fractions of solvent and solute respectively. Extending this to a solution of a polydisperse sample we can write

$${}_sK_{mix} = {}_sK_1\ w_1 + \sum_{i=1}^{\infty} {}_sK_{2i}\ w_{2i} \qquad (2.17)$$

where w_{2i} is the weight fraction of the i^{th} fraction of the molecular weight distribution, based on the total weight of the solution,

$$w_{2i} = \frac{m_{2i}}{m_1 + \sum_{i=1}^{\infty} m_{2i}} \qquad (2.18)$$

where m is the mass of the respective species. ${}_sK_{mix}$ is also related to the experimentally measured quantities by

$${}_sK_{mix} = {}_sK_1\ w_1 + {}_sK_2{}^{exp}\ w_2{}^{exp} \qquad (2.19)$$

Here,

$$w_2{}^{exp} = \sum_{i=1}^{\infty} w_{2i} \qquad (2.20)$$

Equating expressions (2.17) and (2.19), and rearranging we get

$$ {}_sK_2^{exp} = \sum_{i=1}^{\infty} {}_sK_{2i} \frac{w_{2i}}{w_2^{exp}} \qquad (2.21) $$

It follows from equation (2.18) and (2.20) that

$$ {}_sK_2^{exp} = \sum_{i=1}^{\infty} {}_sK_{2i}\, w_i \qquad (2.22) $$

where w_i is the weight fraction of the i^{th} fraction of the molecular weight distribution, based on the total mass of the polymer solute. Hence, the experimentally obtained specific Kerr constant is the weight average of Kerr constants of the individual species. Similarly, it can be shown that the experimentally obtained molecular Kerr constant is a number average Kerr constant.

For monodisperse polymer molecules without any permanent dipole moment, the ratio of the square of optical polarizability anisotropy to the molecular weight is given by[35],

$$ \frac{(\alpha_{||} - \alpha_{\perp})^2}{M} = \frac{405\ kT}{4\pi N_A}\, {}_sK_2 \qquad (2.23) $$

where N_A is the Avogadro number, k the Boltzmann constant, T is the absolute temperature and M the polymer molecular

weight. But since our samples are polydisperse we obtain an average value for the above mentioned ratio from the measured ${}_sK_s{}^{exp}$,

$$\left[\frac{(\alpha_{||} - \alpha_{\perp})^2}{M}\right]_{ave} = \int_0^{\infty} \frac{(\alpha_{\parallel} - \alpha_{\perp})^2}{M} f(n)\, dn \qquad (2.24)$$

For a wormlike chain, combining equation (1.11) and equation (1.12) we get

$$(\alpha_{\parallel} - \alpha_{\perp})^2 = \frac{2}{3}\frac{\varepsilon^2 g_2}{x} n^2 \alpha_o^2 \qquad (2.25)$$

where n is the degree of polymerization and α_o is the mean optical polarizability of a monomer unit. Note that mean polarizability being a scalar quantity, is given by

$$\frac{\alpha_{||} + 2\alpha_{\perp}}{3} = n\ \alpha_o \qquad (2.26)$$

On substituting equation (2.25) and equation (1.19) in equation (2.24), and evaluating the integral we get

$$\left[\frac{(\alpha_{||} - \alpha_{\perp})^2}{M}\right]_{ave} = \frac{2\alpha_o^2\varepsilon^2}{3M_o}\left[\frac{1}{\beta} - \frac{y}{3\beta^2} + \frac{y^2}{3\beta^2(y+3\beta)}\right] \qquad (2.27)$$

where

$$y = \frac{2}{n_w}$$

$$\beta = \frac{M_o}{aM_L}$$

n_w is the weight average degree polymerization, a the persistence length, ε the monomer anisotropy ratio, M_o the monomer molecular weight and M_L the molecular weight per unit contour length of the polymer chain. Equation (2.27) has three unknowns a, n_w and ε, hence two more equations are necessary to calculate these variables. These two equations will be obtained from wide angle light scattering as discussed in the next section.

Wide Angle Light Scattering

When a light beam of electric field E is incident on a material, it induces an electric dipole moment **m**, the magnitude of which is proportional to the polarizability α of the material. Since the frequency of visible light ω is much less than the resonant frequency ω_o of electrons, the intensity of the scattered radiation is dependent on ω, and on ω_o in terms of the polarizability $\alpha = e_o^2/m_o\ \omega_o^2$, where m_o is the mass of an electron of charge e_o. This limiting case is known as the Rayleigh scattering after Lord Rayleigh who used the wavelength dependence of scattered light to explain the blue color of the sky.

In the simple oscillator model of an electron bound to a nucleus, the resonant frequency ω_o is related to the force constant k which holds the electrons in place ($\omega_o = k/m_o$). In general, the distribution of electrons is anisotropic

which results in an anisotropic value for the force constant. The polarizability α is thus a tensor.

$$\mathbf{m} = \alpha \cdot \mathbf{E} \qquad (2.28)$$

For an anisotropic material, there are three principal polarizabilities α_1, α_2 and α_3. In the case of cylindrical symmetry these reduce to α_1 and α_2. Let **i** be the unit vector along the principal axis denoted by subscript 1. The anisotropy of polarizability Δ is then equal to $(\alpha_1 - \alpha_2)$. For this system the induced dipole moment is

$$\mathbf{m} = \Delta \ (\mathbf{i}.\mathbf{E}) \ \mathbf{i} + \alpha_2 \ \mathbf{E} \qquad (2.29)$$

If **s** is the unit vector in the direction of polarization of the scattered light after passing through the analyzer, then the scattering amplitude is given by,

$$E_s = K'(\mathbf{m}.\mathbf{s}) \qquad (2.30)$$

The scattered intensity is obtained from the expression,

$$I_s = K \ (\mathbf{m}.\mathbf{s})^2 \qquad (2.31)$$

Consider the case of scattering of light from vertically polarized incident beam. If the analyzer is horizontal, the scattering geometry is referred to as H_v and the scattering occurs due to the orientation fluctuations in the material. However, if the analyzer is vertical, the geometry is referred to as V_v and the scattering is due to density and orientation fluctuations.

The intensity of the scattered light from anisotropic molecules for the H_v and V_v geometries obtained from equation (2.31) is

$$I_{Hv} = K\ E^2\ \frac{\Delta^2}{15} \qquad (2.32)$$

$$I_{Vv} = K''\ E^2 \left(\alpha_o^2 + \frac{4\Delta^2}{45} \right) \qquad (2.33)$$

where $\alpha_o = (\alpha_1 + 2\alpha_2)/3$.

The isotropic scattering for a system consisting of anisotropic molecules can be obtained by rearranging equation (2.32) and (2.33) as follows :

$$I_{iso} = I_{VV} - \frac{4}{3} I_{HV} \qquad (2.34)$$

The above analysis has an implicit assumption, that the direction of the incident field is not modified in crossing the boundary of the scattering particle. This is known as the "Rayleigh-Gans approximation". This is a good approximation when the particle size is small compared to the wavelength of radiation - X-ray, neutron or light - and the scattering contrast between the particle and its surrounding is not too large. More exact theories have been developed by Mie and others[36,37] to consider cases for which the Rayleigh-Gans approximation is not valid.

Light Scattering from Pure Liquids

In a gas each molecule is randomly positioned in space, hence scattering from these molecules can be considered to be

incoherent. Therefore the sum of scattering intensities from each molecule will give the total scattering from the gas. This is not true for a liquid because the molecules in this case are not completely randomly located in space, but undergo somewhat correlated motion.

The density of a liquid in a given small volume is a randomly fluctuating quantity due to the thermal motion of the molecules with time. Hence the total local density of a liquid can be considered as the sum of the average density of the liquid which is constant throughout the liquid, and the random fluctuation from this mean value. The scattering arises exclusively from the fluctuation of the local density.

Einstein[38] has treated the scattering from liquids using a fluctuation approach to account for the phenomenon of critical opalescence. It is assumed that each volume element has random fluctuations of density and therefore acts as an incoherent scatterer. The total scattering from the liquid is just the addition of scattering from each volume element, like the gas molecules. The fluctuation in density depend on the bulk compressibility of the medium ξ. The scattering caused by the resultant fluctuation in optical polarizability will depend on ξ and the refractive index n. The scattering arising from density fluctuations is thus given by

$$R_{total} = C_F R_d$$

$$R_d = \frac{2\pi^2 n\ kT\ \xi}{\lambda_o{}^4}\left[\rho\left(\frac{dn}{d\rho}\right)_T\right] \qquad (2.35)$$

where k is the Boltzmann constant, λ_o is the wavelength of light in vacuum and ρ is the density of the medium. The quantity from the square brackets can be obtained from the Eykman expression[39,40].

$$\rho\left(\frac{dn}{d\rho}\right)_T = \frac{(n+0.4)(n^2-1)}{(n^2+0.8n+1)} \qquad (2.36)$$

The Cabannes factor C_F in equation (2.35) accounts for the anisotropy of the scattering elements. For vertically polarized light the depolarization ratio, ρ_v, is

$$\rho_v = \frac{I_{HV}}{I_{VV}}$$

and

$$C_F = \frac{R_{total}}{R_{iso}} = \frac{3}{3-4\rho_v} \qquad (2.37)$$

Scattering from pure liquids like benzene or toluene is used to obtain absolute calibration of light scattering instruments.

Light Scattering from Solutions

Light scattering from solution of a polymer in a solvent or a mixture of two liquids arises from density fluctuations (R_d) and from the concentration fluctuations (R_c). These two

components of scattering can be assumed to be independent of each other at low concentrations.

$$R_{iso} = R_c + R_d \qquad (2.38)$$

The scattering from concentration fluctuations is given by

$$R_c = \frac{K\ RT\ c}{(d\tau/dc)_T} \qquad (2.39)$$

where K_L is the light scattering constant given below, c the polymer concentration, R the gas constant and τ the osmotic pressure.

$$K = \frac{4\pi^2 n^2}{\lambda_o{}^4\ N_A} \left(\frac{dn}{dc}\right)^2 \qquad (2.40)$$

where (dn/dc) is the differential refractive index increment, N_A is the Avogadro number and λ_o is the wavelength of the incident light in vacuum.

For dilute polymer solutions, equation (2.39) can be expressed in the well known Zimm form[41]

$$\frac{K\ c}{R_c} = \frac{1}{M\ P(q)} + 2A_2\ c + \ldots \qquad (2.41)$$

with

$$q = \frac{4\pi n}{\lambda_o} \mathrm{Sin}(\theta/2)$$

P(q) is the intramolecular interference factor, θ is the scattering angle, M the polymer molecular weight and A_2 is the second virial coefficient. For monodisperse Gaussian

coils consisting of isotropic scattering segments, P(q) is given by the well known Debye equation,

$$P(q) = \frac{2}{u}\left[e^{-u} - 1 + u\right] \qquad (2.42)$$

where $u = R_g^2 q^2$.

For small values of q, that is $u < 1$

$$\frac{K\,c}{R(q)} = \frac{1}{M}\left[1 + \frac{Rg^2}{3}\,q^2 + O(q^4)\right] \qquad (2.43)$$

Note that this equation is valid irrespective of the shape of the particle- rod, sphere or coil.

Light Scattering from Stiff Chains

This has been treated by Nagai[27] for monodisperse wormlike polymer chains consisting of anisotropic scattering segments. The Porod-Kratky chain is considered to have a contour length L and a persistent length a. The chain is assumed to have three principal optical polarizabilities per unit length, α_1 along the contour and α_2 along the two directions perpendicular to the contour, that is the chain is assumed to have a cylindrical symmetry. A lower symmetry with $\alpha_2 \neq \alpha_3$ is not practical for this model. $\alpha_o = (\alpha_1+2\alpha_2)/3$ and $\Delta\alpha = (\alpha_1-\alpha_2)$ are the mean and anisotropic polarizabilities per unit length of the chain. The depolarized scattering is given by

$$\frac{R_{HV}}{KcM} = \left[\frac{2}{45}\frac{\varepsilon^2 g_2}{x}\right] - \left[\frac{11}{5670}\frac{a^2\varepsilon^2 g_4}{x}\right] q^2 \qquad (2.44a)$$

$$\frac{R_{VV}}{KcM} = \left[\frac{8}{135}\frac{\varepsilon^2 g_2}{x} + 1\right] - \left[\frac{4}{135} a^2 \varepsilon g_3 - \frac{x\, a^2\, g_1}{9}\right] q^2 \qquad (2.44b)$$

where

$$x = L/a$$

$$\varepsilon = \Delta\alpha/\alpha_o$$

$$g_1(x) = 1 - \frac{3}{x} + \frac{6}{x^2} - \frac{6}{x^3} + \frac{6}{x^3} e^{-x} \qquad (2.45a)$$

$$g_2(x) = 1 - \frac{1}{3x} + \frac{1}{3x} e^{-3x} \qquad (2.45b)$$

$$g_3(x) = 1 - \frac{4(42+\varepsilon)}{63}\frac{1}{x} + \frac{(1638+51\varepsilon)}{567}\frac{1}{x^2} - \frac{(30+\varepsilon)}{10x^2} e^{-x} + \frac{(42+5\varepsilon)}{378x^2} e^{-3x}$$
$$- \frac{\varepsilon}{63x} e^{-3x} - \frac{\varepsilon}{315x^2} e^{-6x} \qquad (2.45c)$$

$$g_4(x) = 1 - \frac{971}{66x} + \frac{189}{110x} e^{-x} - \frac{19}{66x} e^{-3x} + \frac{1}{11} e^{-3x} + \frac{13}{330x} e^{-6x}$$

(2.45d)

-

The total scattered intensity, R_{Uv}, is given by

$$\frac{R_{UV}}{K\ c\ M} = A_1 + A_2\, q^2 \qquad (2.46)$$

where

$$A_1 = 1 + \frac{14}{135}\frac{\varepsilon^2 g_2}{x} \qquad (2.47a)$$

$$A_2 = \frac{4}{135} a^2 \varepsilon g_3 - \frac{x\, a^2\, g_1}{9} - \frac{11}{5670} \frac{a^2 \varepsilon^2 g_4}{x} \qquad (2.47b)$$

Rearranging equation (2.46) to get the scattering equation in the conventional Zimm form, we get

$$\frac{K\,c}{R(q)} = \frac{1}{MA_1}\left[\, 1 \; - \; \frac{A_2}{A_1} q^2 + O(q^4)\right] \qquad (2.48a)$$

$$M_{app} = MA_1 \qquad (2.48b)$$

$$R^2_{gapp} = - \frac{3A_2}{A_1} \qquad (2.48c)$$

Polydispersity Correction

Our polymer samples were synthesized by a polycondensation reaction between a diamine and a diacid chloride. Hence the samples are polydisperse with the molecular weight distribution being approximated by the most probable distribution. Zimm[42] has derived the following relation for scattered intensity from a polydisperse system of polymer chains, as the sum of intensities from each scattering species.

$$\frac{R(q)}{KcM_o} = \int_0^\infty n\, f(n)\, P(q)\, dn \qquad (2.49)$$

where M_o is the monomer molecular weight and n is the degree of polymerization.

As an example let us consider the case of polydisperse Gaussian coils. In this case for small values of q the intramolecular interference factor is given by,

$$P(q) = 1 - \frac{R_g^2}{3} q^2 \qquad (2.50)$$

In fact the above equation is valid for particles of any shape. Solving equation (2.49) with this value of P(q) and rearranging, we get

$$\frac{K\ c}{R(q)} = \frac{1}{M_w}\left[\ 1 + \frac{\langle R_g^2\rangle_z}{3} q^2 + \ldots.\right] \qquad (2.51)$$

M_w is the weight average molecular weight and $\langle R_g^2\rangle_z$ is the z-average radius of gyration.

For polydisperse stiff anisotropic chains P(q) is given by

$$P(q) = A_1 + A_2\ q^2 \qquad (2.52)$$

where A_1 and A_2 are defined by equation.(2.47). Inserting equation.(2.52) in equation.(2.49), and evaluating the resulting Gamma functions we obtain

$$\frac{K\ c}{R(q)} = \frac{1}{M\underline{A}}\left[\ 1 \ - \ \frac{\underline{B}}{\underline{A}} q^2 + O(q^4)\right] \qquad (2.53)$$

where

$$\underline{A} = \frac{2}{y} + \frac{14\varepsilon^2}{135}\left[\frac{1}{\beta} - \frac{y}{3\beta^2} + \frac{y^2}{3\beta^2(y+3\beta)}\right] \qquad (2.54a)$$

$$\beta = \frac{M_O}{aM_L} \qquad (2.54b)$$

$$\underline{B} = \frac{4a^2\varepsilon}{135}(G3) - \frac{a^2}{9}(G1) - \frac{11a^2\varepsilon^2}{5670}(G4) \qquad (2.55a)$$

$$G1 = \frac{6\beta}{y^2} - \frac{6}{y} + \frac{6}{\beta} - \frac{6y}{\beta^2} + \frac{6y^2}{\beta^2(y+\beta)} \qquad (2.55b)$$

$$G3 = \frac{2}{y} - \frac{4(42+\varepsilon)}{63\beta} + \frac{(1638+51\varepsilon)y}{567\beta^2} - \frac{(30+\varepsilon)y^2}{10\beta^2(y+\beta)} + \frac{(42+5\varepsilon)y^2}{378\beta^2(y+3\beta)} - \frac{\varepsilon y^2}{63\beta(y+3\beta)^2} + \frac{\varepsilon y^2}{315\beta^2(y+6\beta)} \qquad (2.55c)$$

$$G4 = \frac{1}{\beta} - \frac{97y}{66\beta^2} - \frac{189y^2}{110\beta^2(y+\beta)} - \frac{19y^2}{66\beta^2(y+3\beta)} + \frac{y^2}{11\beta(y+3\beta)^2} + \frac{13y^2}{330\beta^2(y+6\beta)} \qquad (2.55d)$$

M_L is molecular weight per unit contour length. The apparent molecular weight and radius of gyration are thus given by

$$M_{app} = M_O \underline{A} \qquad (2.56a)$$

$$R^2_{gapp} = -3\frac{\underline{B}}{\underline{A}} \qquad (2.56b)$$

The above two equations have three unknowns: persistence length a, monomer anisotropy ratio ε and number average degree of polymerization n_w. The above two equations along with equation (2.27) from Kerr effect experiment can be solved simultaneously to obtain the solution.

Depolarized Light Scattering

In the theory of light scattering from polymer molecules we assume that a polymer chain consist of a linear sequence of small identical optical segments which behave as independent scattering centers. If the segment is isotropic, the light scattered at 90° with reference to the direction of the incident light is entirely vertically plane polarized since anisotropic orientation fluctuations are absent. Polymer molecules consisting of optically anisotropic segments do exhibit some depolarization effect when the incident light is either vertically polarized or unpolarized. The ratio of the horizontal component to the vertical component of the scattered light is known as the depolarization ratio.

$$\rho_v = \frac{R_{Hv}(90°)}{R_{Vv}(90°)} \qquad (2.57)$$

This ratio characterizes the optical anisotropy of the molecule.

Let us now consider the effect of large size and polydispersity on the light scattering from polymer solutions. It is usually expected that $Kc/R(\theta)$ versus q^2 lines in Zimm plots for large size chains, that is $R_g^2q^2 > 1$, should curve upward. But in case of polydisperse polymer

samples, these curves are linear even for $R_g^2q^2 > 1$ due to the compensating effect of sample polydispersity as shown in Figure 8.

Let us investigate this effect for polydisperse Gaussian coils. The intramolecular interference factor P(q) for Gaussian coils is given by equation (2.42). Evaluating the Zimm equation (2.49) for polydisperse system with P(q) given by equation (2.58) we get

$$\frac{K\,c}{R(q)} = \frac{1}{M_w}\left[\,1 + \frac{\langle R_g^2\rangle_w}{2}\,q^2\,\right] \qquad (2.58)$$

where $\langle R_g^2\rangle_w$ is the weight average square of the radius of gyration. The above equation is same as equation (2.51) since $2\langle R_g^2\rangle_z = 3\,\langle R_g^2\rangle_w$ for most probable distribution. Note that equation (2.58) is valid for any value of $R_g^2q^2$. Hence one obtains a linear fit even for $R_g^2q^2 > 1$.

Equation (2.58) holds for Gaussian coils consisting of isotropic scattering elements. It is desirable to obtain a similar equation for Gaussian chains made up of anisotropic segments. The theory for this case has been developed by Utiyama and Kurata[43,44],

$$\frac{R_{Hv}}{KcM} = \frac{3}{5}\,\zeta^2 \qquad (2.59a)$$

$$\frac{R_{Vv}}{KcM} = \frac{4}{5}\zeta^2 + P(q) \qquad (2.59b)$$

where P(q) is given by equation (2.58). Substituting equation (2.58) and equation (1.12) in the above two equations, and accounting for polydispersity using equation (2.49) we get,

$$\frac{R_{Hv}}{KcM_o} = \frac{2}{45}\varepsilon^2(G2) \qquad (2.60a)$$

$$\frac{R_{Vv}}{KcM_o} = \frac{8}{135}\varepsilon^2(G2) + \frac{2}{\frac{2}{n_w} + \frac{b^2\beta}{12}q^2} \qquad (2.60b)$$

where

$$G2 = \frac{1}{\beta} - \frac{y}{3\beta^2} + \frac{y^2}{3\beta^2(y+3\beta)} \qquad (2.60c)$$

b is the Kuhn step length and q is the magnitude of the scattering vector.

This equation is valid only for Gaussian coils, that is for L/a --> ∞. Due to lack of any better light scattering theory which is valid for $R_g^2q^2 > 1$ we will use equation (2.60) to calculate the depolarization ratio theoretically.

Another set of equations can be obtained from Nagai's theory which is valid for $R_g^2q^2 < 1$. Correcting equation (2.44) for polydispersity we obtain,

$$\frac{R_{HV}}{KcM_o} = \left[\frac{2\varepsilon^2}{45}(G2)\right] - \left[\frac{11}{5670}\, a^2\varepsilon^2(G4)\right] q^2 \qquad (2.61a)$$

$$\frac{R_{VV}}{KcM_o} = \left[\frac{2}{y} + \frac{8}{135}\varepsilon^2(G2)\right] - \left[\frac{4a^2\varepsilon}{135}(G3) - \frac{a^2}{9}(G1)\right] q^2 \qquad (2.61b)$$

where G1, G2, G3 and G4 are functions of y and β. Note that equation (2.61) is valid for a wormlike chains (that is for any value of L/a) with $R_g^2 q^2 < 1$. Equation (2.60) and equation (2.61) will be used to interpret experimental data of Rayleigh ratios and depolarization ratios from Depolarized light scattering experiments.

Differential Refractometry

The Dale-Gladstone relation for differential refractive index increment in terms of polymer refractive index n_2 and specific volume V_2 is

$$\frac{dn}{dc} = V_2 \, (n_2 - n_1) \qquad (2.62)$$

where n_1 is the solvent refractive index. Knowing the (dn/dc) values for a given polymer in two different solvents we can calculate n_2 and V_2 for that polymer. The mean optical polarizability of the structural unit is calculated using the Lorentz-Lorenz equation,

$$\frac{(n_2^2-1)}{(n_2^2+1)} = \frac{4\pi}{3} N_p \alpha_0 \qquad (2.63)$$

where N_p is the number density of submolecules with mean polarizability α_o.

Intrinsic Viscosity

The hydrodynamics of Gaussian polymer molecules has been considered by Kirkwood and Riseman[45]. The polymer molecule is modeled as a string of touching beads which act as point friction sources. The intrinsic viscosity according to this theory is given by

$$[\eta] = \phi \frac{< R^2>_o^{3/2}}{M} \qquad (2.64)$$

where $< R^2>_o$ is the unperturbed mean square end-to-end distance and M is the molecular weight. Auer and Gardner[46] value of ϕ is 2.87×10^{23} mole^{-1}. Rewriting equation(2.64) in terms of Kuhn step length b and contour length L gives,

$$[\eta] = \phi \frac{(L\ b)^{3/2}}{M} \qquad (2.65)$$

Equation (2.65) is derived for a flexible chain assuming the Kuhn step length to be comparable to the chain diameter.

In order to generalize equation (2.65) for a semiflexible chain, we have to incorporate the following:

a) chain stiffness leading to nongaussian statistics

b) local friction sources which are cylinder-like with length b.

Just as in the case of the excluded volume effect[47], the chain stiffness is incorporated as a renormalized Kuhn step, b_1 defined by

$$< R^2 > = L\, b_1 \qquad (2.66)$$

For a wormlike chain model,

$$< R^2 > = b^2 \left[\frac{L}{b} - \frac{1}{2} + \frac{1}{2} e^{-2L/b} \right] \qquad (2.67)$$

Here the Kuhn step length b is equal to twice the persistence length a. Using equation(2.67) in equation(2.66),

$$b_1 = b \left[1 - \frac{b}{2L} (1 - e^{-2L/b}) \right] \qquad (2.68)$$

where b is the Kuhn step of the corresponding Gaussian coil.

The hydrodynamics of a rigid rod polymer consisting of (2p+1) beads with the diameter D equal to the step length b has been treated by Muthukumar and Hatziavramidis[48]. The intrinsic viscosity according to this theory is given by

$$[\eta] = \left(\frac{\pi N_A}{24\ \ln(p)} \right) \frac{L^3}{M} \qquad (2.69)$$

where L = 2pb. This is the same result[49,50] as that of Riseman-Kirkwood-Auer in the non-free draining limit. Rewriting equation(2.69) in terms of $<R^2>$ we obtain

$$[\eta] = \left(\frac{\pi N_A}{24\ \ln(p)}\right) \frac{< R^2 >^{3/2}}{M} \qquad (2.70)$$

For a semiflexible chain,

$$p = \frac{b_1}{2D} \qquad (2.71)$$

since the friction at the local scale can be approximated by that from a cylinder of length b_1 and the diameter D of the beads. Using the prefactor of equation(2.70) with p given by equation(2.71) to incorporate this local friction, we obtain an approximate expression for the intrinsic viscosity,

$$[\eta] \approx \left(\frac{\pi N_A}{24\ \ln(b_1/2D)}\right) \frac{(L\ b_1)^{3/2}}{M} \qquad (2.72)$$

It is important to note that according to the above equation the prefactor for a Gaussian coil with persistence length greater than the chain diameter (a >> D) will not be 2.87 X 10^{23} $mole^{-1}$, but will be given by prefactor of equation (2.72). Hence equation (2.64) is valid only for a Gaussian chain with persistence length approximately equal to the chain diameter.

The theory for intrinsic viscosity of stiff chains without excluded volume has also been developed by Yamakawa and Fuji[51], using the Oseen-Burgers procedure of hydrodynamics for wormlike cylinder model. According to this theory the intrinsic viscosity for semiflexible chains with (L/b) $\geq$ 2.278 is given by

$$[\eta] = \left(\frac{\phi}{1 - \sum_{i=1}^{4} C_i \left(\frac{L}{b}\right)^{-i/2}} \right) \frac{(L\ b)^{3/2}}{M} \qquad (2.73a)$$

The coefficients C_i are independent of L but depend on the diameter D of the wormlike cylinder. For $(D/b) \leq 0.1$ the coefficients C_i are

$$C_1 = 3.230981 - 143.7458\left(\frac{D}{b}\right) - 1906.263\left(\frac{D}{b}\right)^2 + \left[2.463404 - 1422.067\left(\frac{D}{b}\right)^2\right] \ln\left(\frac{D}{b}\right)$$

$$C_2 = -22.46149 + 1347.079\left(\frac{D}{b}\right) + 19387.400\left(\frac{D}{b}\right)^2 + \left[-5.318869 + 13868.57\left(\frac{D}{b}\right)^2\right] \ln\left(\frac{D}{b}\right)$$

$$C_3 = 54.81690 - 3235.401\left(\frac{D}{b}\right) - 49357.06\left(\frac{D}{b}\right)^2 + \left[15.41744 - 34447.63\left(\frac{D}{b}\right)^2\right] \ln\left(\frac{D}{b}\right)$$

$$C_4 = -32.91952 + 2306.793\left(\frac{D}{b}\right) + 36732.64\left(\frac{D}{b}\right)^2 + \left[-8.516339 + 25198.11\left(\frac{D}{b}\right)^2\right] \ln\left(\frac{D}{b}\right) \qquad (2.73b)$$

A stiff chain with any D/b ratio becomes a Gaussain coil when the contour length L becomes very large. According to equation (2.73) as $L \to \infty$ the prefactor is given by 2.87×10^{23} for any $D/b \leq 0.1$. It is interesting to note that this is contrary to our result from equation (2.72), since for example, the prefactor for a Gaussain coil with $D/b = 0.1$ is 0.49×10^{23} mole^{-1}, about six times lower than ϕ.

Equation (2.72) and (2.73) is convoluted with the most probable distribution function to obtain the experimental intrinsic viscosity,

$$[\eta]_{expt} = \int_0^\infty [\eta]\ ny^2\ e^{-yn}\ dn \qquad (2.74)$$

This integral has been evaluated numerically to obtain persistence length, a, which is the only unknown in equation (2.74).

Small Angle X-ray and Neutron Scattering

The small angle scattering from a very long, infinitely thin, irregularly coiled chain molecule (wormlike chain) is composed of three parts as shown in Figure 9a[52]. The coils as a whole gives rise to a scattering effect at very small angles which is shaped roughly like a Gaussian curve. At somewhat larger scattering angles scattering occurs from sections of the molecule which represents a random arrangement of scattering masses, leading to a $1/q^2$ behavior. At still larger angles scattering occurs from smaller and smaller sections of the macromolecule and eventually approaches the behavior of a rod, that is $1/q$ dependence.

In the Kratky-Porod plot of Iq^2 versus q the second range is a horizontal line and the third region is a straight line with a positive slope and its extrapolation passes through the origin as illustrated in Figure 9b. The intersection of these two regions is the transition point from which the persistence length, a, can be directly determined by

$$a = \frac{2.3}{q^*} \qquad (2.75)$$

When the coils are not very large, the effect is as shown in Figure 10. The middle branch of the curve is not horizontal but has a positive slope. The smaller the molecule, larger is the slope and eventually it approaches the slope of the third region.

The persistence length can also be ascertained from the smeared data I^s, without the need for slit desmearing. In this case a plot of $\frac{dI^s}{dq}q$ against q gives a transition point which agrees within a few percent of q^*. The radius of gyration can be obtained from a Guinier plot of lnI versus q^2 for low angles. The slope of this plot is given by

$$\text{Slope} = -\frac{R_g^2}{3}$$

Furthermore, the mass per unit length can be determined from the slope of the third region in the Kratky-Porod plot. It should be noted that we are primarily concerned with the persistence of direction and not persistence of curvature.

CHAPTER 3

EXPERIMENTAL

Kerr Effect

To determine the induced birefringence a plane polarized beam of light is sent through the medium in a direction perpendicular to the electric field E, with its plane of polarization at an angle of 45^0 relative to E. The probe beam can be resolved into two plane polarized beams of equal amplitude, one with a polarization parallel to E and the other perpendicular to E. Each beam experiences a different refractive index as is passes through the birefringent medium. Thus the difference in velocity of each beam will make the resultant beam elliptically polarized. The optical retardance δ between the two beams which is related to the birefringence by[53]

$$\delta = \frac{2\pi\ L\ \Delta n}{\lambda} \qquad (3.1)$$

where L is length of the birefringent medium and λ is wavelength of probe radiation. An analyzer is placed crossed with the polarizer, at the end of the birefringent medium so that it extinguishes the probe beam in the absence of birefringence. The intensity I emerging through the analyzer in the presence of birefringence is given by[53]

$$\frac{I}{I_o} = \sin^2\left(\frac{\delta}{2}\right) \approx \frac{\delta^2}{4} \qquad (3.2)$$

where I_o is the incident intensity and the approximation holds for small δ.

Consider the case when the induced birefringence is smaller than the background birefringence in the optical components. We therefore have

$$\frac{I}{I_o} = \frac{(b + \delta)^2}{4} \qquad (3.3)$$

If the inducing field is sinusoidal at low frequency then

$$\delta = \delta_o \cos^2\omega t.$$

Substituting this in equation (3.3) it can be shown that[4]

$$\frac{I}{I_o} = \frac{\left(b^2 + b\,\delta_o + \frac{3}{8}\,\delta_o^2 \right)^2}{4} + \frac{\left(b\,\delta_o + \frac{1}{2}\,\delta_o^2 \right)^2}{4} \cos 2\omega t + \frac{1}{64}\,\delta_o^2 \cos 4\omega t \qquad (3.4)$$

The induced birefringence can be measured by using a lock-in amplifier tuned to the 4ω signal which is independent of the background birefringence. For weaker induced birefringences a few percent of third harmonic distortion in the high voltage power supply creates an interfering term at 4ω which depends on the background birefringence.

This limitation is overcome by using a null technique[54] as illustrated in Figure 11. In this case a second Kerr cell with a substance of known Kerr constant of the same sign as the sample Kerr constant is placed in the optical path before the second polarizer with its plate at 90° with respect to first cell (Figure 11b). If the Kerr constants are of opposite sign the reference cell is placed so that its electrode plates are parallel to the sample cell electrodes. For these two cases the total retardance of the light after passing through the crossed polarizers is given by

$$\delta = \delta_1 \pm \delta_2 + b \qquad (3.5)$$

Substituting this in equation (3.2) and retaining only the 2ω component of the modulated light beam we have

$$\frac{I(2\omega)}{I_o} \sim (1-e)\ (\delta_1 \pm \delta_2 + b)\ (\delta_1 \pm \delta_2)\ \mathrm{Cos}2\omega t \qquad (3.6)$$

where e is the ratio of the intensity of light transmitted through the plane polarizer to that of the incident wave polarized perpendicular to the optic axis of the polarizer. The null conditions according to the above equation are illustrated in Figure 11b and Figure 11c. Note that since (1-e) appears as a factor in the amplitude of the output intensity modulated at 2ω, the Kerr constant obtained by the null technique is independent of the polarizer efficiency.

Experimentally a sinusoidal voltage is applied to the reference cell to compensate for the retardation created by

the sample cell. The null condition can be detected at 2ω as is seen from equation (3.6). High sensitivity (10^{-6} radian) can be attained with this technique. The Kerr constant for the unknown sample can be determined by

$$B_{sample} = B_{ref} \frac{l_{ref}}{l_{sample}} \left(\frac{V_{ref}/d_{ref}}{V_{sample}/d_{sample}} \right)^2 \qquad (3.7)$$

where l_{ref} and l_{sample} are the lengths of the cells. d_{ref} and d_{sample} are electrode spacings of the two cells. In our experiment, cell length and electrode spacings are identical for the two cells, hence the Kerr constant is given by

$$B_{sample} = B_{ref} \left(\frac{V_{ref}}{V_{sample}} \right)^2 \qquad (3.8)$$

The experimental apparatus for measurement of Kerr constants is shown in Figure 12. The probe beam is a 10 mW He-Ne red laser (Melles Griot, Model 05LHP 991) with beam diameter 0.68 mm. Red light is chosen since our samples (polyamide as well as polysilane) absorb in the ultraviolet region. The plane polarizers are polarizer sheets from Polaroid corporation.

The cell electrodes are stainless steel plates with dimensions 2 cm X 10 cm X 0.8 cm. These will be separated by Teflon spacers 3mm thick. Both the cells are made of glass, with a cooling / heating jacket and condensation free optical

windows to conduct low temperature studies. The detector used was a silicon photodiode (Oriel Corporation, Model 7182). The sinusoidal signal of 10 volt peak at 140 Hz from the signal generator (Wavetek, Model 75) was amplified by an audio power amplifier to 420 V peak. The power amplifier was built using two power operational amplifiers (APEX μTech, Model PA85) driven by a ± 220 volt DC power supply (Kikusui Electronics Corp., Model PAB350-0.2). A schematic circuit diagram of the power amplifier is given in the appendix. The output of the power amplifier was fed to a 1:10 step up transformer (Gavagan Electronics, Model 8540) to provide 4.2 kV peak across each electrode assembly. The voltages across each cell were varied independently by adjusting the output of the signal generator between 0 to 10 V peak. The phase difference between the voltage signals applied to the two cells was reduced to zero by the phase adjust option of a Tektronix Model 2232 digital oscilloscope. The signal from the detector is fed to a phase sensitive amplifier (Stanford Research Systems, Inc., Model SR510) locked in at twice the frequency of the reference signal from the signal generator. High Voltages were measured using a 1000:1 probe and a Hewlett Packard Model 3478A digital voltmeter. The reference liquid used was CS_2. The Kerr constant B_{ref} of CS_2 at required temperatures was obtained from the International critical tables[55].

Experimental Challenges

In case of low temperature studies of polysilanes it is essential to avoid condensation of moisture on the Kerr cell windows. This was achieved by constructing double walled windows. The space between the double wall was filled with dry N_2.

The solvent used for polyamide studies was THF. The polyamide samples under study form aggregates by H-bonding even if small amounts of moisture is present in the system. This is due to the amide moiety. The experimental evidence regarding this aggregation process will be discussed in chapter 4. Nonetheless, in order to get a true molecularly dispersed solutions anhydrous THF (Aldrich Chemical Co.) with water content less than 0.005% was used. All solutions were prepared, stored and transferred to sample cells in a sealed glove bag purged with nitrogen dried over drierite. The glove bag was purged 6-7 times after each transfer of material from outside the bag to the inside.

Tetrahydrofuran is a very corrosive solvent and was found to attack all commercially available O-ring materials like viton etc. We used custom made Teflon O-rings to circumvent this problem.

Due to the high voltages applied in the Kerr effect experiment, it was found that it was necessary to keep the electrical conductivity of the solvent less than 0.1 (Mohm-cm)$^{-1}$ to avoid electric shorting of the high voltage circuit. In order to achieve such low electrical conductivity solvent should be free of acidic/basic impurities. Amongst the solvents in which the polyamide sample is soluble - acetone, tetramethylurea (TMU), dimethyl acetamide (DMAc), dimethyl foramide (DMF), tetrahydrofuran (THF) - only THF was readily available in 99.9% purity from Aldrich Chemical Co.. The solvent choice was also governed by its inertness to the insulation and coatings coming in contact with the solvent. For example, TMU, DMAc and DMF are highly corrosive and attack PVC coatings of insulated wires and enamel coatings of copper wires. THF is very inert towards these insulating materials.

Electric fields used in the Kerr effect experiments are about 10 to 15 kV/cm. Hence it is necessary to have electromagnetic shielding of high voltage transformers to avoid electrical interference. Sheilding was achieved by enclosing the transformer in a metal casing which was grounded. The reference signal to the lock-in amplifier was maintained at 1 V rms using a potentiometer to ensure optimum operation.

Electric birefringence, Δn, of 10^{-9} has been routinely measured by our apparatus for polyamide in THF, as will be discussed in the next chapter. This gives an idea of the sensitivity of the experiment.

We have been routinely able to reproduce the literature values of Kerr constants of different solvents within reasonable experimental error, as is evident from Table 1. Another experiment that we carried out with the aim of checking the validity of our apparatus was Kerr effect of PBLG in dichloroethane. PBLG is known to assume a helical conformation in Dichloroethane at room temperature. Figure 13 shows the variation of electric birefringence, Δn with E^2 for PBLG in dichloroethane at 24 °C. The data obeys Kerr law at low field strengths but shows saturation at higher fields. At low fields the molecule follows Boltzmann statistics since $\mu E/kT<<1$, where μ is the permanent dipole moment of the molecule, E is the electric field strength, k is the Boltzmann constant and T is the absolute temperature. Hence in the limiting case of weak field, E --> 0, the molecules obey Kerr law. On the other hand, in the limiting case of high field, E --> ∞, thermal energy cannot perturb the molecules aligned along the electric field ($\mu E/kT>>1$) and hence the induced birefringence saturates to a limiting value.

O'Konski[56] has considered the theory of a rigid rodlike molecule with a permanent dipole moment, μ, along the axis of the particle. According to this theory, in the weak field case ($\mu E/kT<<1$) the induced birefringence is given as

$$\Delta n = \frac{\Delta n_s}{15}\left[\frac{\mu^2}{kT}\right] E^2 - \frac{2\ \Delta n_s}{315}\left[\frac{\mu}{kT}\right]^4 E^4 \qquad (3.9)$$

where k is the Boltzmann constant, T the absolute temperature and Δn_s the limiting birefringence reached at very high fields. It is clear that a plot of $\Delta n/E^2$ versus E^2 should be a straight line at low enough fields. Such a plot for our experimental data for PBLG/DCE is shown in Figure 14. The dipole moment of PBLG molecule calculated from the slope and the intercept of this plot is compared with that obtained by O'Konski[56] in Table 2. As is evident, the dipole moment calculated is in excellent agreement with O'Konski's value. The specific Kerr constants, ${}_sK_2$, are slightly different due to the different wavelength of light used to make the measurement. Note that the Kerr constant is dependent on wavelength, but the dipole moment is independent of wavelength.

Light Scattering

Conventional light sources like Hg lamps etc were used in early light scattering experiments. Nowadays lasers have

taken place of these sources. Lasers can provide well collimated, intense and monochromatic beams. The experiments in this work include wide angle light scattering (WALS) and depolarized light scattering.

Wide Angle Light Scattering

These experiments were performed in Prof. Hoagland's laboratory. The instrument used is the SOFICA light scattering apparatus. The light source is a polarized He-Ne laser(1), which provides a beam at 633 nm. The plane of polarization of this laser is adjusted so that it is vertical as shown in Figure 15. The beam passes through an adjustable slit (2) and a principal lens (3) before being incident on the sample cell. The sample cell (5) is a 1 inch diameter pyrex glass vial containing the polymer solution. The sample cell is sealed using Teflon tape inside a dry bag to prevent moisture from contaminating the polymer solution. The sample cell is held in a thermostated glass vat (4) which contains excess xylene to minimize stray light, by means of a sample holder. The scattered beam is steered by a pair of entrance and exit slits (6,9) and total reflection prisms (7,10) onto the detector which is a photomultiplier tube (12). The detector signal is read off a Keithley digital voltmeter.

The detector is mounted on an arm which can be rotated about the sample position. The nominal scattering angles

accessible are from 26° to 150°. Absolute intensity measurements are performed using the scattering from pure toluene for calibration. The main beam is prevented from entering the detector by using a light trap (8). A manual shutter (11) used to protect the photomultiplier tube when the instrument is not in use. The validity of the instrument was checked by reproducing weight average molecular weight, z-average radius of gyration and second virial coefficient of polystyrene standard in toluene.

Depolarized Light Scattering

Depolarized light scattering experiments were performed in the physics department in Professor Langley's laboratory. The instrument used is basically a quasi-elastic light scattering apparatus which can be used for total intensity light scattering measurements also. The source is a spectra Physics 165 Ar Ion laser, which provides a beam with wavelength of 515 and 488 nm. The beam passes through a polarizer and a beam monitor, before being incident on the sample. The sample is held in a thermostated glass vat which contains excess toluene to minimize stray light. If necessary the beam can be focussed onto the sample using a lens before the vat. The scattered beam then passes through an analyzer, a pair of slits and onto the detector which is a photomultiplier tube. The photomultiplier tube is connected to a photon counter through an amplifier-discriminator. The

photon counter is connected to a Langley Ford digital correlator which is run off a Tektronix computer. A schematic diagram of such a instrument is shown in Figure 16.

The detector is mounted on an arm which can be rotated about the sample position. The nominal scattering angles accessible are from 30° to 135°. Absolute intensity measurements are performed using the scattering from pure toluene for calibration. To calculate depolarization ratio we require only the relative intensities. Pure solvents and solutions were studied using 10 mm diameter pyrex glass test tubes. Intensity readings were recorded for 10 different positions of the test tube for both Hv and Vv configurations. The mean of these readings was considered for the final calculation of depolarization ratio,

$$\rho_v = \frac{I_{HV}^{soln}(90°) - I_{HV}^{solv}(90°)}{I_{VV}^{soln}(90°) - I_{VV}^{solv}(90°)} \qquad (3.10)$$

where superscript soln and solv stand for solution and solvent.

Differential refractive index increments (dn/dc) at 633 nm were measured with a chromatix (LDC Milton Roy) KMX-16 differential refractometer. The KMX-16 was calibrated with aqueous sodium chloride solutions (dn/dc = 0.174 at 633 nm at 25 °C).

The intrinsic viscosity, [η], of polyamide in THF was measured with a Cannon Ubbelohde viscometer immersed in a constant temperature bath maintained at 31 °C. [η] was determined by extrapolation of the reduced viscosity, η_{sp}/c to infinite dilution, using the Huggins relation

$$\frac{\eta_{sp}}{c} = \frac{\eta_{rel}-1}{c} = [\eta] + k_H [\eta]^2 c + \ldots.$$

with $\eta_{rel} = \eta/\eta_o$ where η and η_o are the viscosities of the solution and solvent respectively.

SAXS and SANS

SAXS experiments were conducted at the SUNY beamline of the National Synchrotron Light Source, Brookhaven National Laboratory. The X-rays were collimated by use of a modified Kratky system described elsewhere[57]. The wavelength of the radiation was 1.54 Å and the beam size at the sample surface was 1 x 2 mm. Solutions of Poly(di-n-hexyl silane) in Hexane were studied using glass capillaries of 1.5 mm diameter and 0.01 mm glass thickness. The small angle scattered intensity was collected by a linear position sensitive photo diode array coupled to an Optical Multichannel Analyzer System (Princeton Applied Research). Data were corrected for detector dark current, background and sample absorption.

Small angle neutron scattering from poly(di-n-hexyl silane)/Hexane solutions was conducted at the Small angle diffractometer at the Intense Pulsed Neutron Source, Argonne National Laboratory.

CHAPTER 4

RESULTS AND DISCUSSION

Kerr Effect

Poly(di-n-hexyl silane)

Kerr constant of poly(di-n-hexyl silane) (M_w = 1 X 10^6) in hexane were determined for solutions with concentrations ranging from 0.25 to 1.5 mg/ml. Each solution was also studied at various temperatures from 45° to -25°C.

The specific Kerr constant $(B-B_o)/c$ for this polymer was found to be about 5 x 10^{-7} cm^4/SV^2 gm at room temperature. It was found to be constant over the temperature range 45° to 5°C, within the experimental error. Also the Kerr constant does not show any concentration dependence from 0.25 to 1.5 mg/ml.

When cooled to low temperature, all the solutions gave noisy birefringence signal around -5°C. This may be due to aggregate formation prior to eventual precipitation at about -25°C. A precipitate was observed as a milky white gel blocking the laser beam completely. Hence we conclude that the low temperature transition in polysilanes is not accessible by Kerr effect experiment, due to the lack of

enough birefringence signal at low concentrations (0.02mg/ml) necessary to keep the molecules in solution.

Polyamide

The chemical structure of the paralinked aromatic polyamide studied is shown in Figure 1. Three samples TA61, TA62 and TA63 with different molecular weights were used for this study. Their exact molecular weights will be ascertained by combining the Kerr effect data and the wide angle light scattering data.

The electric birefringence experiment was performed on four solutions of each sample, with increasing concentration in THF. For each such solution null technique was used to balance the retardation over a range of electric field from about 5 to 10 kV/cm to establish linear Kerr law in each case. Figure 17 shows Δn plotted against square of the electric field for pure solvent (THF) and for a 1.0 mg/ml solution. The Kerr law is obeyed in both cases shown. The induced electric birefringence of THF is negative and becomes positive upon addition of polyamide to the pure solvent. This means that the net birefringence will be zero at some concentration between 0 and 1.0 mg/ml. Hence it is desirable to perform the experiment over a concentration range before concluding about the Kerr effect of a given polymer sample. It is obvious that the Kerr effect of polyamide must be

positive since it increases Δn of THF. The reason for the negative sign of the Kerr constant for THF has been explained in detail in chapter 2. The slope of the lines in Figure 17 is the Kerr constant (B) of the solution and B_1 of the solvent. The excess Kerr constant, $B-B_1$, is plotted as a function of polyamide weight fraction, w_2, in Figure 18 for samples TA61, TA62 and TA63. From these curves we conclude that molecular weight of TA62, TA61 and TA63 should decrease in that order. The initial slope of these lines is the constant a_4 in equation (2.10)

The specific Kerr constant at infinite dilution ${}_sK_2$ is calculated using equation (2.6). In our case it was found that a_1, a_2 and a_3 are negligible compared to a_4. Hence ${}_sK_2$ is given by

$$ {}_sK_2 = {}_sK_1 \ (1 + a_4) \qquad (4.1) $$

This experimental value of ${}_sK_2$ gives an average value of $[(\alpha_{\parallel} - \alpha_{\perp})^2/M]_{ave}$ due to polydispersity of the samples according to equation (2.23). Equation (2.27) will be used in the next section along with the two WALS equations to calculate the unknowns - persistence length a, weight average degree of polymerization n_w and monomer optical anisotropy ratio ε.

Electric birefringence experiments were also performed to study the effect of temperature on Kerr constant of the polyamide solution. Figure 19 shows the variation of specific Kerr constant ${}_sK_2$ for sample TA61, TA62 and TA 63

over a temperature range from 10° to 50°C. As the temperature increases, ${}_sK_2$ decreases approximately linearly. Since for a given sample ${}_sK_2$ is directly proportional to $(\alpha_{||} - \alpha_{\perp})^2$, there is a decrease in optical anisotropy of the whole chain with temperature. At higher temperatures there is rotation of adjacent groups making the chain more coil-like or flexible, hence decreasing its optical anisotropy.

In order to evaluate the effect of moisture on the Kerr constant, we performed electric birefringence experiments on samples contaminated with known amounts of water. Results of these experiments are shown in Figure 20. The lower line is for Kerr constant of pure THF with different quantities of water added to it. Theoretically calculated Kerr constant of these solutions, using the Kerr constant of water and THF, is also shown. The experimental value agree very well with theory. This serves to illustrate two important points. Firstly, it indicates the amount of experimental error involved in these experiments. Secondly, the increase in Kerr constant seen in the upper curve for TA62 solution is actually due to changes in the polyamide structure rather than excess water itself. The increase in specific Kerr constant of TA62 and TA63 solution upon addition of water is shown in Figure 21. There is no change in the Kerr constant within experimental error until about 0.1% excess H_2O. Above this concentration of water there is a distinct increase, indicating aggregation of molecules due to H-bonding. These

experiments clearly indicate that it is extremely important to keep the solution free of moisture in order to prevent aggregate formation. Water molecules form a bridge between two polyamide molecules to form aggregates.

Wide Angle Light Scattering

Wide angle light scattering was measured with SOFICA light scattering instrument. Data for sample TA63, TA61 and TA 62 is plotted in form of conventional Zimm plot of $Kc/R(\theta)$ versus $Sin^2(\theta/2)$ + 2000c as shown in Figure 22,23 and 24 respectively. The molecular weight and radius of gyration obtained from these plots are apparent quantities due to the anisotropic nature of the scattering segments. The parameters M_{app}, R_{gapp} and A_{2app} were determined by extrapolation of $Kc/R(\theta)$ to c=0 and θ=0 as indicated by the relation

$$\frac{Kc}{R(\theta)} = \frac{1}{M_{app}} \left(1 + 2A_{2app}c + ..\right) \left(1 + \frac{q^2R^2_{gapp}}{3} + ..\right) \quad (4.2)$$

$R(\theta)$ is the Rayleigh factor at scattering angle θ, c is the concentration in gm/ml.

The theory to relate M_{app} and R_{gapp} to molecular parameters has been developed in chapter 2. This theory is a modification of the light scattering theory developed by

Nagai[27] for persistent wormlike polymer chain, to incorporate polydispersity effect. Equation (2.56a) and (2.56b) from WALS and equation (2.27) from electric birefringence experiment have been solved numerically on a computer for the unknown molecular parameters a, ε and n_w. The degree of polymerization n_w, persistence length a and monomer anisotropy ratio ε calculated from WALS and Kerr effect measurements are listed in Table 3.

The persistence length and the monomer anisotropy ratio are independent of molecular weight within the experimental error indicating that wormlike chain model can successfully represent the real chain. The apparent and true molecular weights and radii of gyration are also given in Table 3. Sample TA61 and TA62 both have fairly similar molecular weights within experimental error. But the root mean square z-average radius of gyration R_{gz} of TA62 is larger than that of TA61, hence TA62 is the highest molecular weight sample. The apparent second virial coefficient obtained has not been corrected for optical anisotropy due to the lack of any theory dealing with this. Fractional chain extension is quite high indicating the semiflexible nature of these polyamides. Note that this ratio approaches unity for a rigid rod, and is equal to $1/\sqrt{n_k}$ for a Gaussian coil with n_k Kuhn statistical segments.

In the previous section we established that aggregates of polyamide are formed on addition of water. This is as expected since H_2O molecule can form a bridge between two amide groups by H-bonding. In addition, we have now conclusively established that no aggregates of 2,2'-disubstituted biphenyl polyamides are formed in THF provided the system is kept moisture free ($H_2O < 0.005\%$). This is surprising since THF has a low dielectric constant, and hence cannot successfully reduce the attractive electrostatic forces between the H atom and O atom of the two amide group intending to form a H-bond. Moreover, this behavior is unlike single phenyl polyamides like Kevlar, which form H-bonds very easily. These hydrogen bonds cannot be broken by low dielectric constant solvent like THF and hence are soluble only in strong acids.

The explanation of this observation lies in the chemical structure of the polyamide we are studying. In 2,2'-disubstituted biphenyl polyamides, hydrogen bonding is expected to be weakened as a result of non-coplanar phenyl rings. For example, in single phenyl polyamides, all of the amide groups lie in the same line, and the phenyl rings rotate out of the plane of amide group by 30° (Figure 25), thus allowing an intermolecular hydrogen bond distance of approximately 3 Å[50] (bond energy = 7 kcal/mol[58]). The hydrogen-bond distance is increased to 7 Å for biphenyl polyamide chains lying parallel to each other according to

molecular models. Moreover, the chance of amide groups coming in exact juxtaposition to form hydrogen bonds with adjacent polyamide chains is very small since amide groups are not coplanar, unlike in the case of single phenyl polyamides.

Depolarized Light Scattering

Depolarization ratio, $\rho = R_{Hv}/R_{Vv}$ was measured at 90°. depolarization ratio at infinite dilution is obtained by extrapolation to zero concentration as shown in Figure 26. These extrapolated values are reported in Table 5. We have also studied a model compound, synthesized to mimic the chemical structure of the paralinked aromatic polyamide repeat unit. Chemical structure of this compound is shown in Figure 27. The depolarization ratio (Figure 28) will be used in the next section to calculate the monomer anisotropy, ε of the model compound.

Before comparing experimental data with the theory of depolarized light scattering, let us have a closer look at the WALS data. The critical angle, θ_{cr}, at which $R_g^2q^2 = 1$ is listed for each sample in Table 4. But in Zimm plots for all samples we observe straight line behavior till 150° as opposed to the expected upward curvature for $R_g^2q^2 < 1$. This is due to the compensating effect of sample polydispersity as

discussed earlier in the depolarized light scattering section of chapter 2.

The results for depolarization ratio ρ_v and reduced Rayleigh ratio (R/kcM_o) from experiments are compared with theory discussed in chapter 2 in Table 5 and Table 6. To recapitulate, we discussed two cases to calculate depolarization ratios and Rayleigh ratios theoretically. Equation (2.60) is valid for Gaussian coils (that is $L/a \rightarrow \infty$) and for any value of q, while equation (2.61) is valid for any value of L/a but with $R_g^2q^2 < 1$.

As is evident from Table 5 and Table 6, Rayleigh ratio and depolarization ratio calculated from equation (2.61) for TA63 are in good agreement with the experimental values. This is expected since $R_g^2q^2 < 1$ at 90° for TA63 as pointed out earlier. The reduced Rayleigh ratio for TA61 and TA62 are grossly underestimated by equation (2.61) due to the neglect of higher order terms in q. This is also reflected in the unreasonably high values of depolarization ratios calculated from equation (2.61).

The Rayleigh ratios have been overestimated by equation (2.60). We should keep in mind that even though equation (2.60) is good for any value of $R_g^2q^2$, it is strictly valid only for Gaussian coils ($L/a >>> 500$). Due to larger Rayleigh ratios the depolarization ratios are consistently

lower than the experimental values, and the agreement improves for largest molecular weight sample TA62. The agreement between theory and experiment is reasonable considering the approximations made in deriving equation (2.60) and equation (2.60). The above discussion points out the significance of the contribution of chain stiffness and the resulting optical anisotropy to depolarization ratios.

Differential Refractometry

Differential refractive index increments (dn/dc) at 632.8 nm were measured with a Chromatix (LDC Milton Roy) KMX-16 differential refractometer. Figures 29 gives the plots used to evaluate dn/dc values for all the three samples. The dn/dc values for TA61, TA62 and TA63 in THF are within experimental error, and the mean value is listed in Table 7. dn/dc measured in TMU, and that for the model compound in THF are also reported.

The Dale-Gladstone relation gives differential refractive index increment in terms of the polymer refractive index n_2, specific volume V_2 and the solvent refractive index n_1. Using the $\frac{dn}{dc}$ values for TA 63 in THF and TMU we get $n_2 = 1.67 \pm 0.03$ and density = 2.00 ± 0.12 gm/ml. Our density value can be compared with that of other fluorinated polymers, like for example poly(tetrafluoroethylene) which has a density of

2.280 to 2.290 gm/ml for as polymerized sample, and 2.302 gm/ml for crystalline sample[59].. The mean optical polarizability of the structural unit is calculated using the Lorentz-Lorenz equation.

The results of these calculations are listed in Table 8. The mean polarizabilities of the polymer are in good agreement with the model compound. The monomer anisotropy, ε, is calculated from the depolarization ratio measured at 515 nm, using the relation

$$\rho_v = \frac{\varepsilon^2}{15 + \frac{4}{3}\varepsilon^2} \qquad (4.3)$$

Equation (4.3) is valid only for small molecules. We have assumed the wavelength dependence of optical polarizabilities to be negligible between 633 nm and 515 nm, since these wavelengths are far removed from the absorption region of the model compound (UV region).

The refractive index and mean polarizability for the polyamide and the model compound are in excellent agreement while the optical anisotropy and ε are not in agreement. This may be due to the model compound forming aggregates in solution, since mean polarizability is independent of aggregation while anisotropy of polarizability is very sensitive to aggregate formation. Note that steric hinderance cannot prevent aggregation since the amide group

of the model compound can be approached from various directions by that of another molecule. The mean polarizability and anisotropy calculated from bond additivity are not in agreement with the experimental data. This is expected since the bond additivity does not hold for molecules with electron delocalization. Table 9 gives refractive indices of various polymers for comparison. The polyamide we studied has a refractive index similar to other rigid polymer molecules.

Intrinsic Viscosity

Intrinsic viscosity in THF was measured with a Cannon Ubbelohde viscometer in a dry box purged with dry nitrogen. The data obtained are plotted in Figure 30 and Figure 31 to evaluate the intrinsic viscosity at 31°C. The plot in Figure 31 is for two different runs for TA61 in THF. This gives an idea about the experimental error involved in these experiments.

The theory of intrinsic viscosity for a semiflexible chain with persistence length a has been discussed in detail in chapter 2. The integral in equation (2.74) has been evaluated numerically for each polyamide sample to obtain the persistence length which is the only unknown in this equation. The persistence length calculated according to Yamakawa-Fujii theory and the approximate hydrodynamic theory

considered in this work is listed in Table 10. The persistence length from our theory is in fairly good agreement with values from light scattering, while that from Yamakawa-Fujii theory is significantly lower than the experimental value. The agreement between light scattering and viscosity results once again confirms that the polyamide studied is molecularly dispersed if the solution is free of moisture.

SAXS and SANS

SANS was performed for solutions of poly(di-n-hexyl silane) in Hexane for 0.3 gm/lit, 4.2 gm/lit and 8.0 gm/lit. Though the amount of scattering increased with concentration, no quantitatively accurate data could be obtained due to low signal to noise ratio. The signal to noise ratio was relatively low even after 6 hrs of data collection, due to the combination of low flux and contrast. This effect was especially significant in the large q region, preventing the evaluation of the persistence length. SAXS experiments performed on poly(di-n-hexyl silane) over similar concentration range also showed insignificant scattering over the solvent background due to low contrast.

CHAPTER 5

CONCLUSIONS AND FUTURE WORK

Conclusions

We will first briefly discuss the agreement between our work and the results from theory and experiments by others. This comparison has been done in Table 11. In order to explain the non-lyotropic behavior of our polymer let us consider the phase behavior of the lyotropic system of rods. This has been treated in detail by Flory[60], Onsager[61] and Ishihara[62]. The same problem for semiflexible chains has been dealt with by odijk[63]. The minimum volume fraction of polymer, v_2, for formation of a stable anisotropic phase is given by

$$v_2 = \frac{k_c}{z} \qquad (5.1)$$

where z is the axial ratio of the rod. In case of semiflexible polymer it would be appropriate to assume that this is given by the ratio of persistence length to diameter of the chain. The values of constant k_c are given in Table 12 for various theories. The last entry in the table has been calculated for the particular case of our polymer sample. To consider the most appropriate case for formation of an anisotropic phase we have used k to be 5.6. The axial ratio for our polymer is about 35, leading to a critical

volume fraction of 48 % w/v. Our polymer precipitates at about 30% w/v. Hence low axial ratio might be one of the reasons for not forming a lyotropic phase. Steric hindrance to close packing due to CF_3 groups may also play an important role.

Refractive index of 1.67 is in good agreement with that for similar polyamides. Both α_o and $(\alpha_1-\alpha_2)$ listed in Table 11 are not in agreement with the bond additivity calculations, since bond additivity does not hold for molecules having electron delocalization.

The aromatic polyamide studied can be satisfactorily modeled as a Kratky-Porod wormlike chain with a persistence length of 220±50 Å and a monomer optical anisotropy ratio of 2.3±0.3. Excluded volume effect seems to be negligible in THF at 25 °C, since the Kratky-Porod model does not include excluded volume interactions.

As discussed earlier, the small axial ratio of 35 may be partly responsible for the fact that the polyamide does not exhibit lyotropic behavior. The repeat unit has high optical polarizability anisotropy, leading to highly birefringent films. It is also conclusively established that no aggregates are formed in THF free of moisture.

The light scattering theory of Nagai and the hydrodynamic theory adopted for semiflexible chains is found to hold very well for the polyamide studied. Based on the agreement between experiment and theory we infer that the molecular weight distribution is of the most probable type. Our depolarized light scattering data indicate that the straight line behavior observed in Zimm plots even for $R_g^2q^2 > 1$, upto $R_g^2q^2$ of about 3.5 is due to the combined effect of polydispersity, large size and anisotropy of the molecule.

Future work

We have calculated the molecular parameters of the polyamide based on our work in a single solvent namely, tetrahydrofuran. We also found that no aggregates are formed in the absence of moisture. It would be interesting to have an additional check on the molecular parameters derived by repeating these experiments in other solvents like TMU, DMAc etc. This will also cast light on the solvent effect in mean polarizability and anisotropy of optical polarizability due to alignment of solvent molecules along a semiflexible chain.

Another suggestion is to study the aggregation process itself by performing wide angle light scattering on solutions with known amount of water added. Studying the radius of gyration as a function of water content will give an idea about the nature and size of aggregates formed.

Reproducibility of these results should indicate the stability of the aggregates. The molecular weight of the aggregates found from wide angle light scattering can be used with Kerr effect results to calculate the optical anisotropy of the aggregates. If the molecules tend to align parallel to each other, then aggregates will have a greater optical anisotropy than the separate molecules. However if the molecules are semiflexible and the aggregate is of appreciable size, the molecules will orient more randomly with respect to each other thus decreasing the optical anisotropy of the aggregate with respect to the algebraic sum of the anisotropy of the constituent molecules. In this way, Kerr effect studies could also probe aggregation, assuming that the solution is sufficiently dilute that equilibrium orientation can be reached during the course of measurements.

The study of the solid state properties of the polyamide studied was beyond the scope of the present work. It would be fruitful to blend these semiflexible chains with a flexible polymer matrix and study the improvement in mechanical properties like modulus and strength due to the stiffness of the filler chains. This would entail blend characterization by FTIR and DSC, and mechanical analysis by DMTA and Instron testing.

Crosslinking this semirigid polyamide to form a network can be achieved by modifying the synthesis of the polyamide.

Such networks can be used to test the validity of rubber elesticity theory for semiflexible chains. The experiment necessary for this study is stress birefringence measurement, in which a film of the network is stretched to various elongation ratios and the resultant macroscopic birefringence is measured using a laser and a babinet compensator. The stress optical coefficient is related to the optical anisotropy of the chain segments and their orientation with respect to each other as described by the rubber elesticity theories. Since we already know the optical anisotropy of a Kuhn step we can follow the orientation of the segments at various elongations.

Lastly, the hydrodynamic theory presented in this work for semiflexible chains is approximate in that the prefactor for the intrinsic viscosity expression is adopted from the theory for rods. A generalized theory which encompasses both Gaussian and rod limits for the prefactor can be developed by solving the equation of motion for a persistent chain consisting of beads with diameter equal to diameter of the chain. The neighboring bead positions are correlated by the persistent length of the chain unlike a Gaussian chain where the bead diameter equals the Kuhn step of the chain.

Table 1 Kerr constants of various solvents.

	B (cm^3/sc^2) T = 25 °C λ=633nm	
Solvent	Our Expt.	Literature*
Cyclo-hexane	4.98×10^{-9}	5.02×10^{-9}
Hexane	5.76×10^{-9}	$>5.0 \times 10^{-9}$
Dioxane	6.37×10^{-9}	6.2×10^{-9}
CCl_4	7.50×10^{-9}	7.7×10^{-9}
Dichloro ethane	5.10×10^{-9}	5.3×10^{-9}

*International critical tables, Vol VII, 1930

Table 2 Permanent dipole moment of PBLG in dichloroethane

	Our Expt	O'Konski[1]
T (^{o}C)	24	28.5
μ (D)	2.6×10^{-3}	2.7×10^{-3}
$_{s}K_{2}$ ($cm^{5}/sV^{2}gm$)	3.0×10^{-6}	3.3×10^{-6}

[1] O' Konski etal., J. Phys. Chem., 63, 1558,1959

Table 3 Molecular Parameters of Polyamide

Sample	n_w	a (Å)	ε
TA 63	170 ± 18	210 ±50	2.0 ± 0.3
TA 61	390 ± 40	210 ± 40	2.5 ± 0.3
TA 62	390 ± 40	230 ± 50	2.6 ±0.4

Sample	M_w	Mapp	A2app (mol cm^3/gm)
TA 63	55,000 ± 6000	57,000 ± 6000	1.0×10^{-3}
TA 61	130,000±14000	138,000±14000	0.6×10^{-3}
TA 62	130,000±13000	140,000±11000	1.3×10^{-3}

Sample	Rgz (Å)	Rgapp (Å)	$\sqrt{R^2}/L$
TA 63	400 ± 50	380 ± 50	0.5
TA 61	600 ± 60	580 ± 60	0.3
TA 62	660 ± 50	630 ± 50	0.3

Table 4 Critical Angle for samples TA61, TA62 and TA63.

Sample	θ_{cr} $(Rq^2q^2=1)$	L/a
TA63	140^{o}	8
TA61	75^{o}	20
TA62	70^{o}	20

Table 5 Comparison of depolarization ratios from WALS with theory for samples TA61, TA62 and TA63.

Sample	ρ_v (expt)	ρ_v (Eq.(2.62))	ρ_v (Eq.(2.61))
TA 63	0.040 ± 0.004	0.028 ± 0.006	0.024 ± 0.006
TA 61	0.038 ± 0.003	0.06 ± 0.03	0.024 ± 0.005
TA 62	0.034 ± 0.003	0.21 ± 0.16	0.025 ± 0.004

Table 6 Comparison of Rayleigh ratios from WALS with theory for samples TA61, TA62 and TA63.

Sample	$\left(\frac{R}{KcM_o}\right)$ (expt)	$\left(\frac{R}{KcM_o}\right)$ (Eq.(2.62))	$\left(\frac{R}{KcM_o}\right)$ (Eq.(2.61))
TA 63	134 ± 21	123 ± 18	144 ± 19
TA 61	250 ± 50	120 ± 70	300 ± 40
TA 62	240 ± 40	90 ± 50	290 ± 30

Table 7 Differential refractive index increments at 633 nm and 25 °C.

Sample	Solvent	$\frac{dn}{dc}$ (ml/gm)
p-aromatic polyamide	THF	0.133 ± 0.004
p-aromatic polyamide	TMU	0.112 ± 0.004
Model Compound	THF	0.151 ± 0.004

Table 8 Optical parameters of Polyamide samples TA61, TA62, TA63 and the model compound.

Sample	n_2	α_o (cm^3) X 10^{23}	ε	$(\alpha_1-\alpha_2)_m$ (cm^3) X10^{23}
Polyamide	1.67±0.03	2.45±0.20	2.4±0.3	5.9 ± 1.3
Model compound	1.71±0.03	2.55±0.19	1.5±0.2	3.8 ± 0.8
Bond Additivity		2.96		1.0

Table 9 Comparison of Refractive Index

Polymer	n_D^{25}
Teflon	1.35
Nylon 6,6	1.53
Poly-sytrene	1.59
PET	1.64
Polyamide studied *	1.67
Polyimide	1.78

*for light of wavelength 633 nm

Table 10 Persistence Length from Viscometry and WALS.

Sample	[η] (ml/gm)	a (Å) (WALS)	a (Å) (Our Theory)	a (Å) (Yamkawa Theory)
TA 63	318 ± 6	210 ± 50	310 ± 30	110 ± 18
TA 61	400 ± 6	210 ± 40	230 ± 12	63 ± 6
TA 62	416 ± 6	230 ± 50	230 ± 10	63 ± 6

Table 11 Comparison of Theory and Experiments

	Our Work	Theory/ Other Work	Comments
LC phase	v_2 > 48% w/v	Precipitate for v_2 > 30%w/v	From Solubility Studies*
n_2	1.67	1.67 - 1.76	For Similar Polyamides*
α_o (cm^3) x 10^{23}	2.45	2.96	From Bond Additivity*
(α_1 - α_2) x 10^{23}	5.9	1.0	From Bond Additivity*

* Rogers, H. G. and et al., Macromolecules, 18, 1058, 1985

Table 12 Value of constant k in equation (5.1) according to various theories

Theory	k_c
Flory	8
Onsager	3.34
Ishihara	3.4
Odijk	5.6

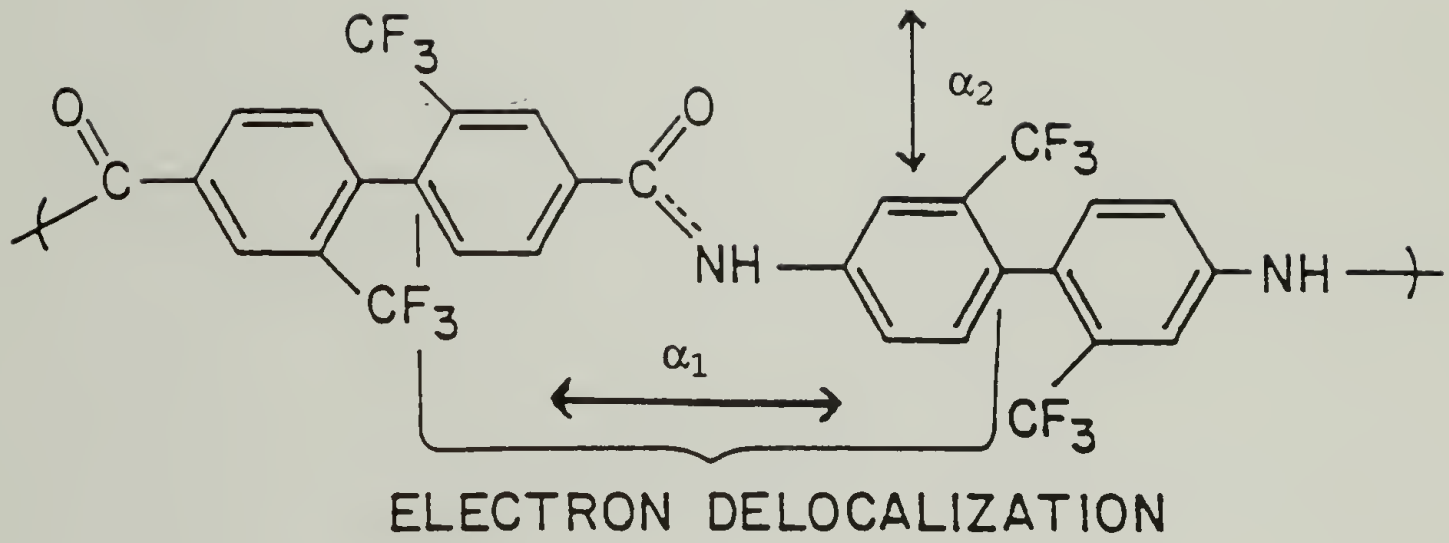

Figure 1 Chemical structure of the paralinked aromatic polyamide used for this study. The extent of electron delocalization is shown. α_1 and α_2 are optical polarizabilities parallel and perpendicular to the polymer backbone.

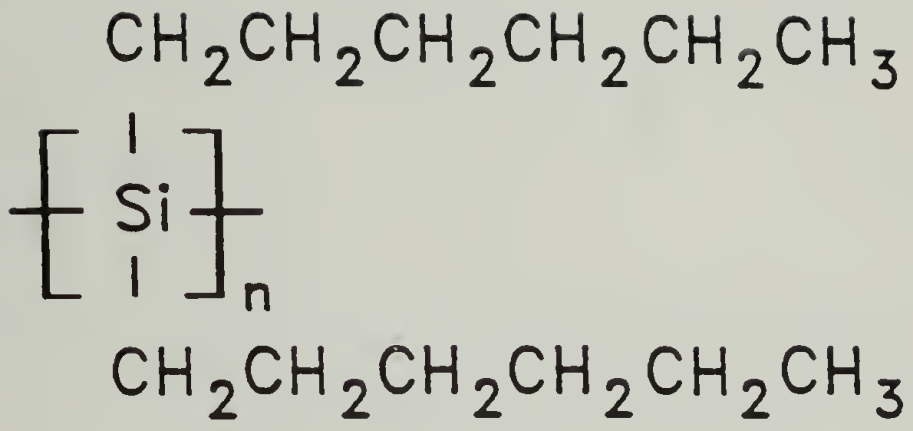

Figure 2 Chemical structure of poly(di-n-hexyl silane).

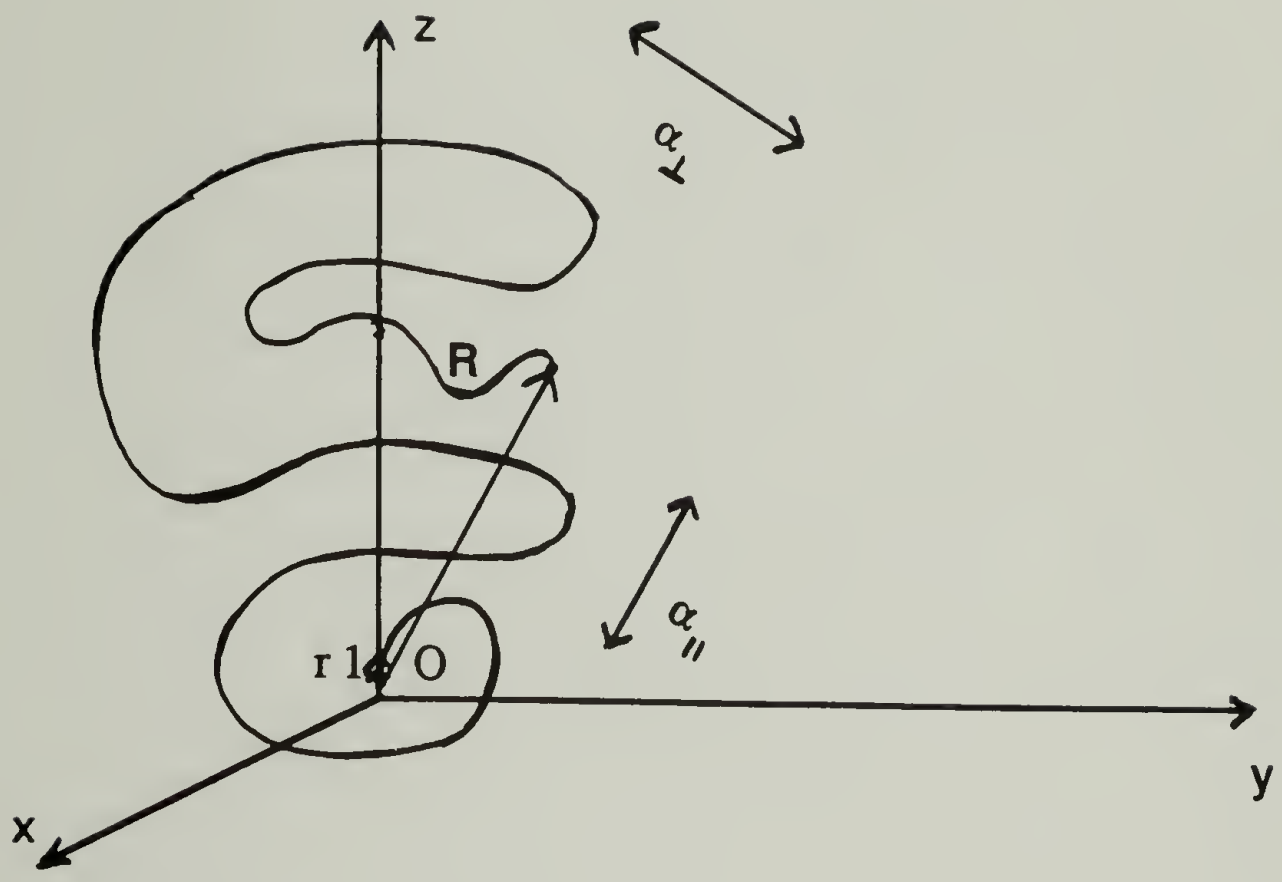

Figure 3 Schematic representation of a persistent chain with its first bond along the z-axis. Optical polarizabilities parallel and perpendicular to end-to-end vector are shown.

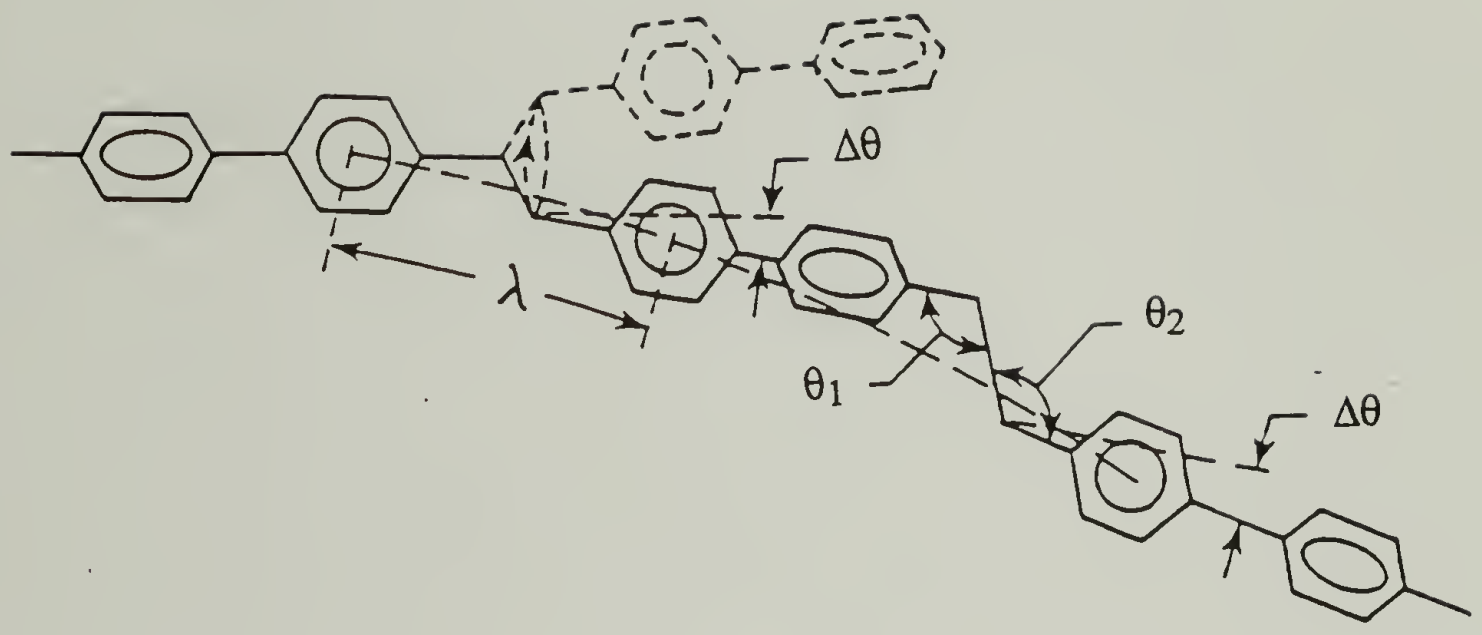

Figure 4 The backbone structure of para-aromatic polyamide showing chain bending $\Delta\theta$ for each monomer step.

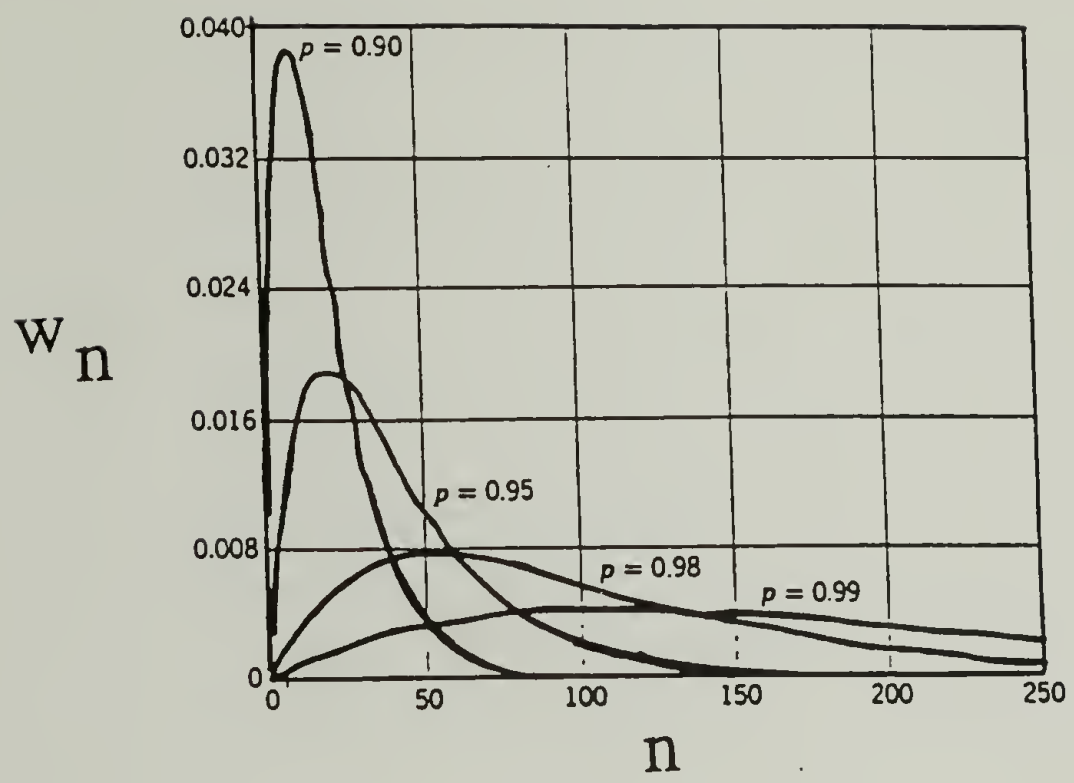

Figure 5 Weight fraction distribution of chain molecules in a linear step-reaction polymer for several extents of reaction *p*.

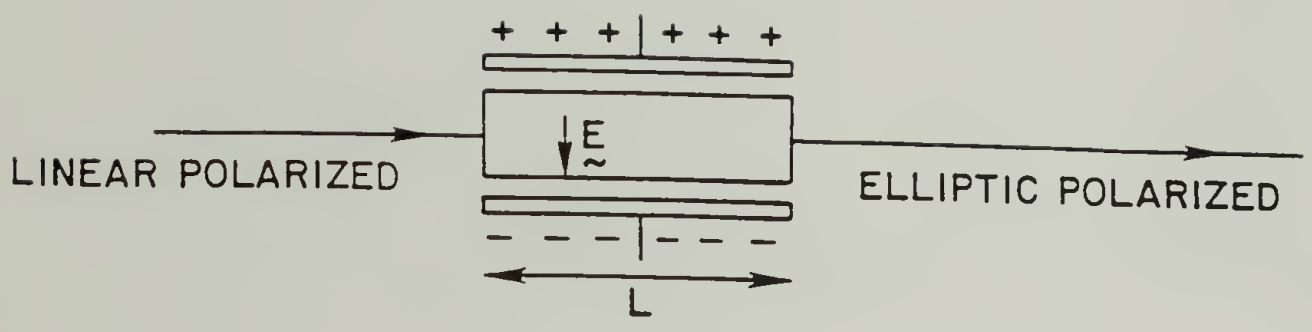

Figure 6 Schematic of a Kerr cell.

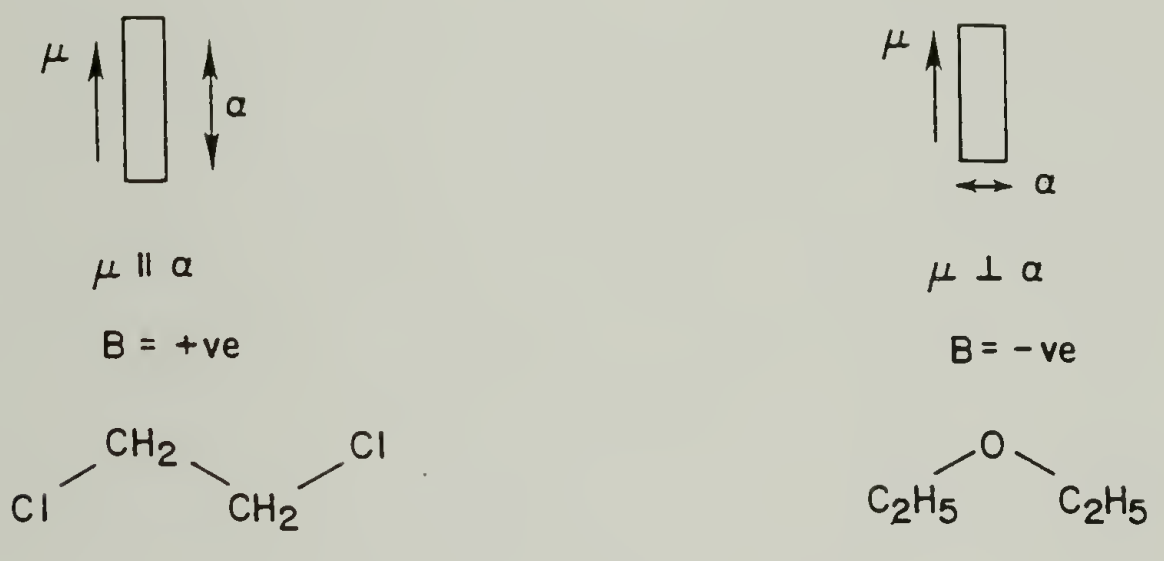

Figure 7 Schematic to illustrate positive and negative Kerr constant

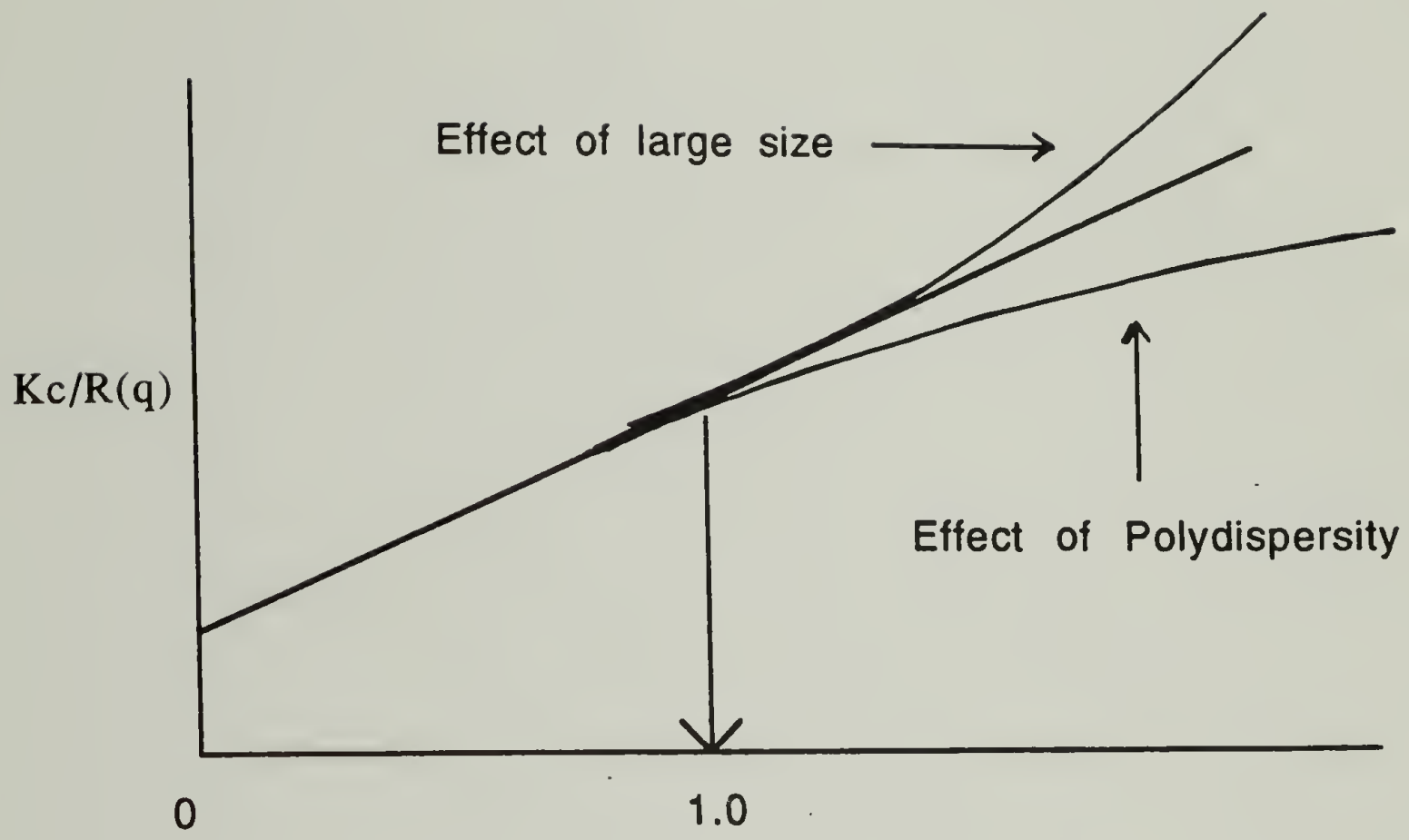

Figure 8 Schematic plot showing effect of large size and polydispersity on angular lines in a Zimm plot.

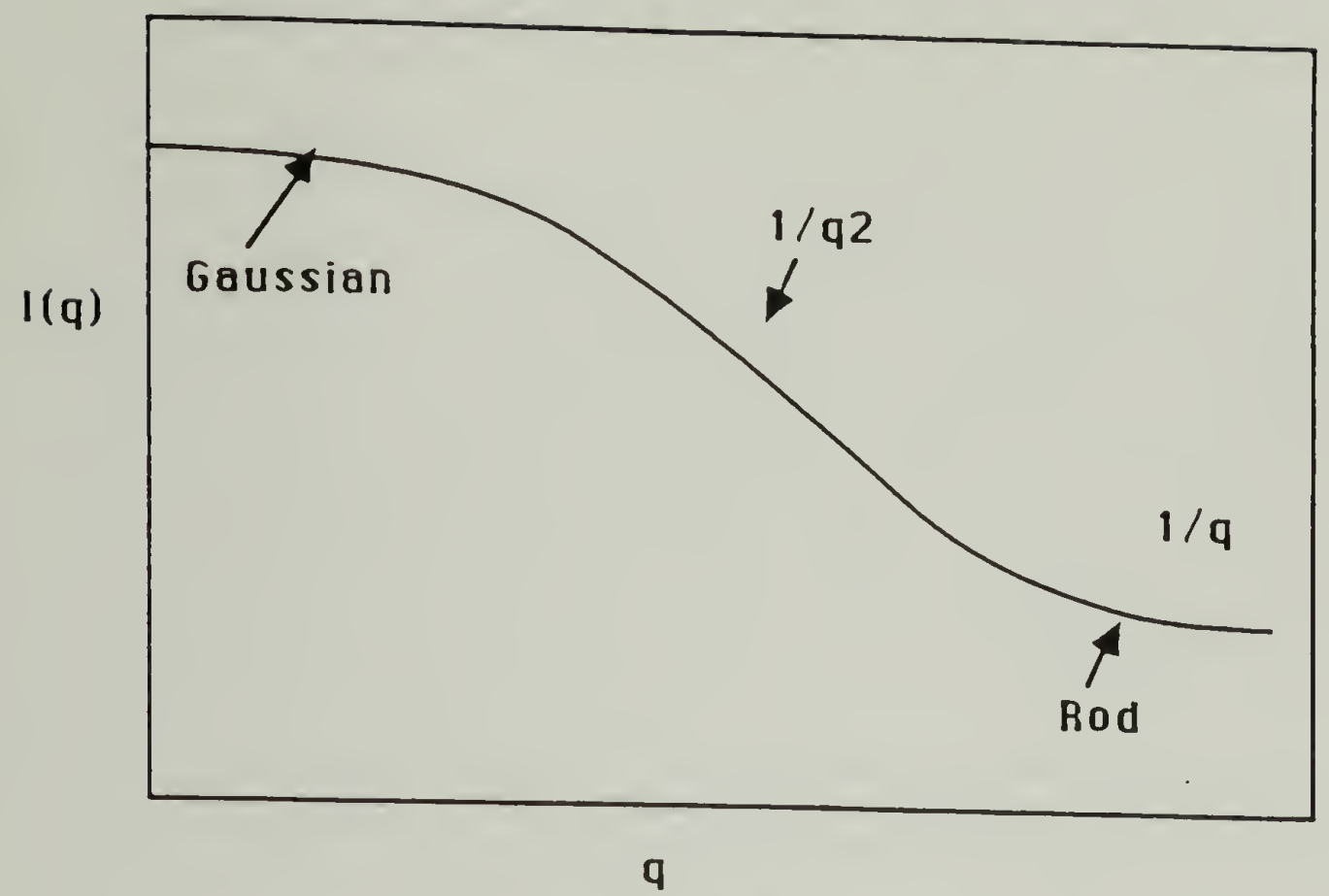

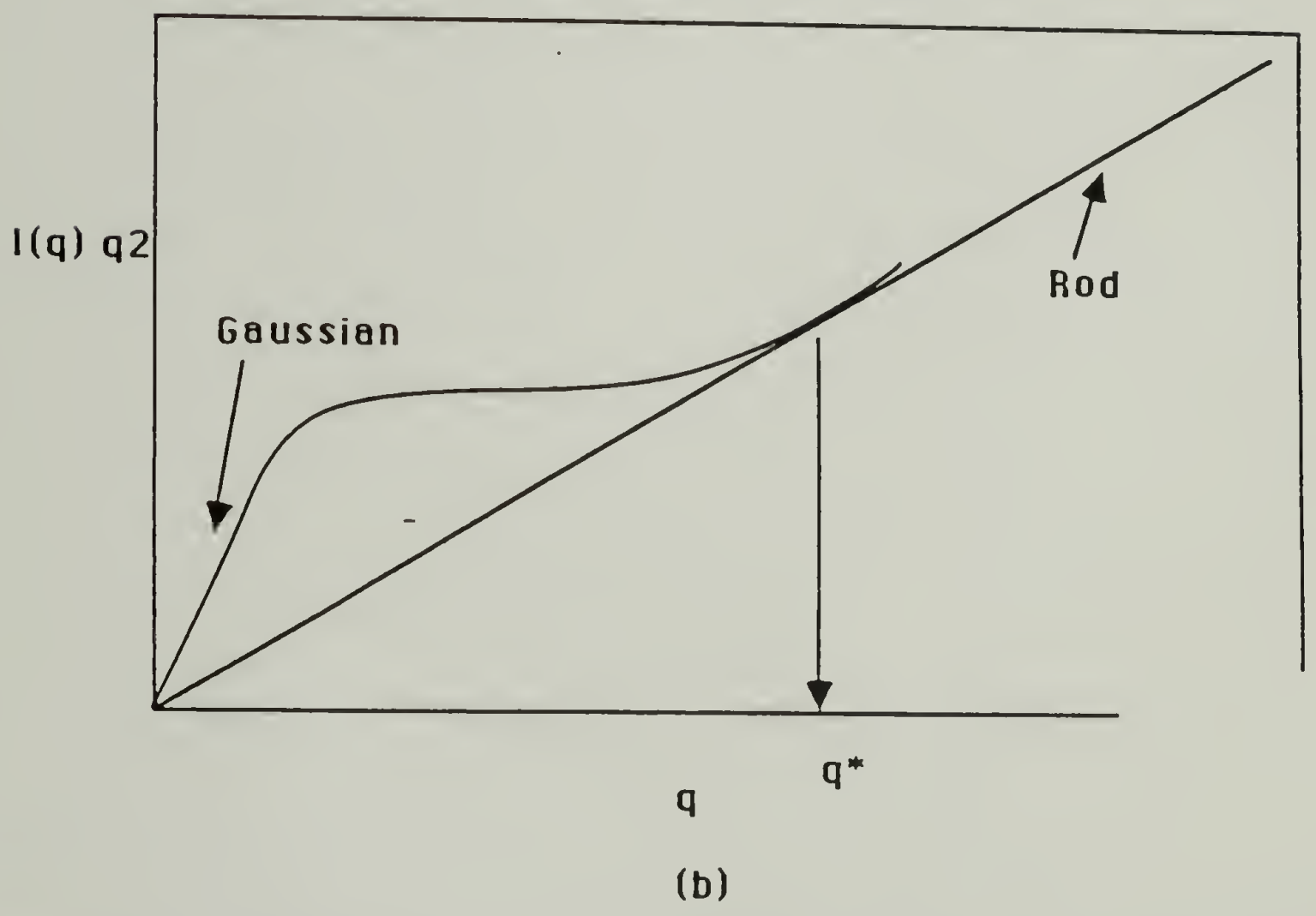

Figure 9 Schematic sketch of the scattering curve of a wormlike chain. (a) Plot of I(q) versus q (b) Plot of I(q) q^2 versus q.

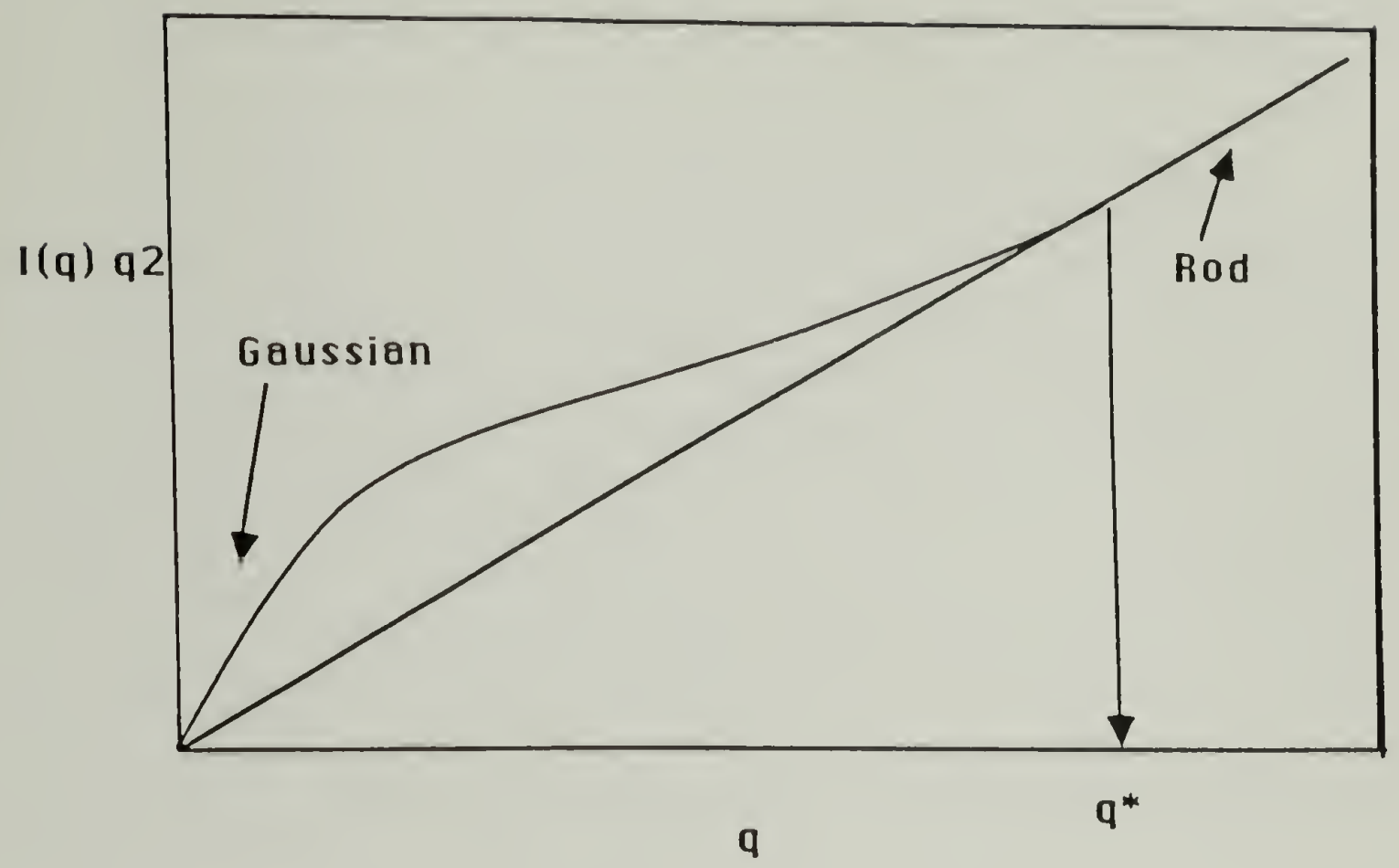

Figure 10 Porod-Kratky plot for a macromolecule with limited number of kuhn steps.

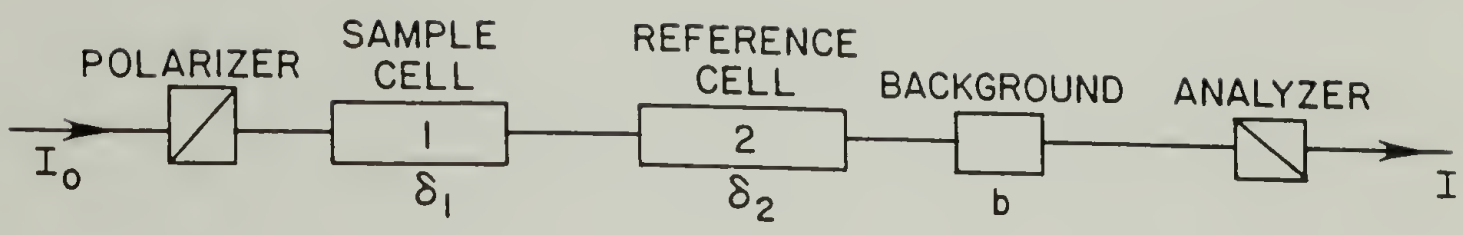

(a)

NULL CONDITION:

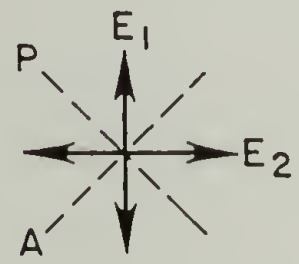

B_1, B_2 SAME SIGN

$\delta_1 - \delta_2 = 0$

(b)

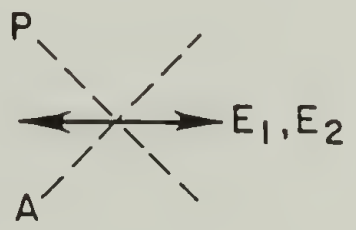

B_1, B_2 OPPOSITE SIGN

$\delta_1 + \delta_2 = 0$

(c)

Figure 11 (a) Schematic of the null technique for retardation measurement. (b) Null condition for reference and sample Kerr constants of same sign, and (c) opposite signs

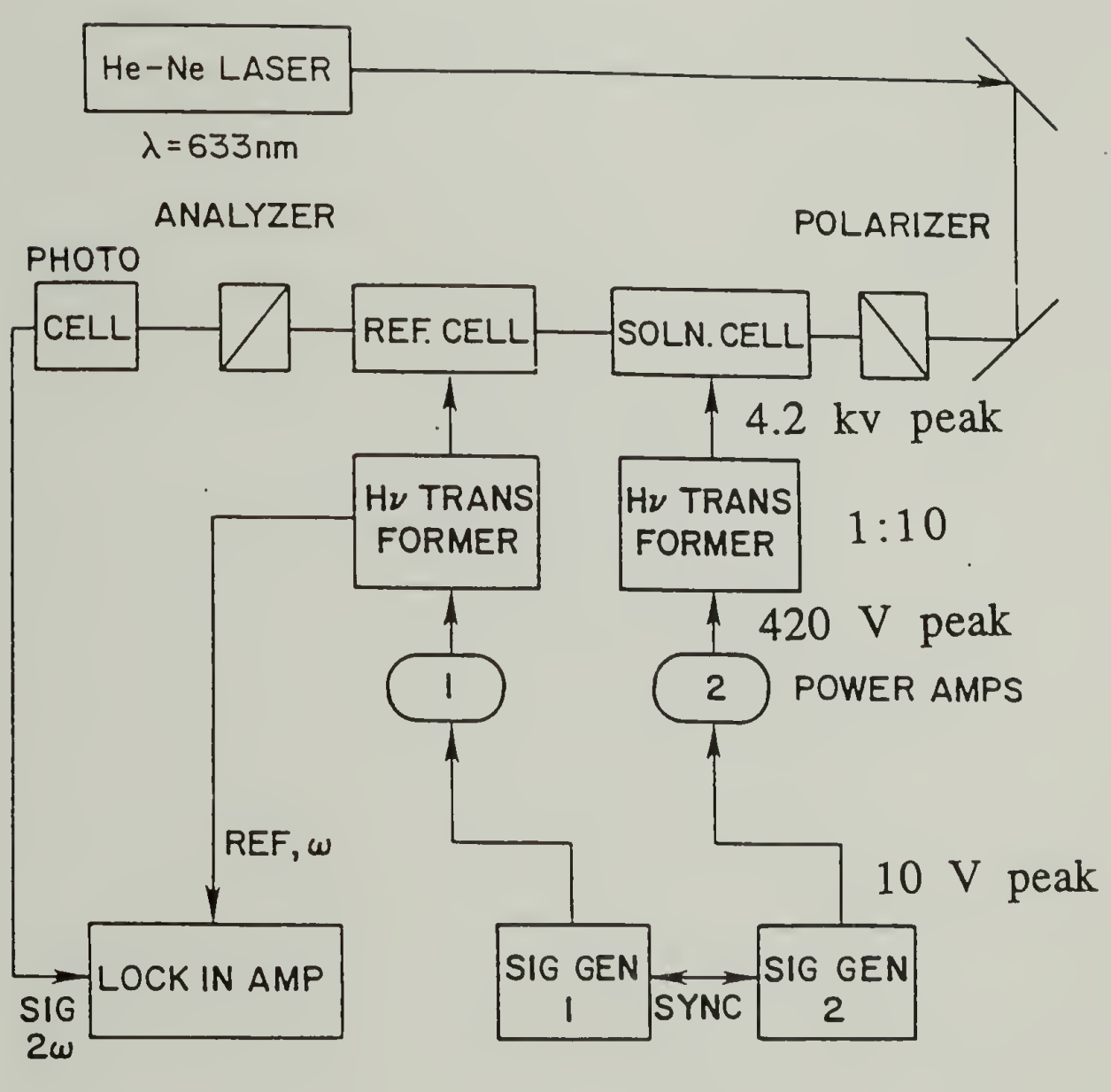

Figure 12 Schematic diagram of the apparatus to measure Kerr constant.

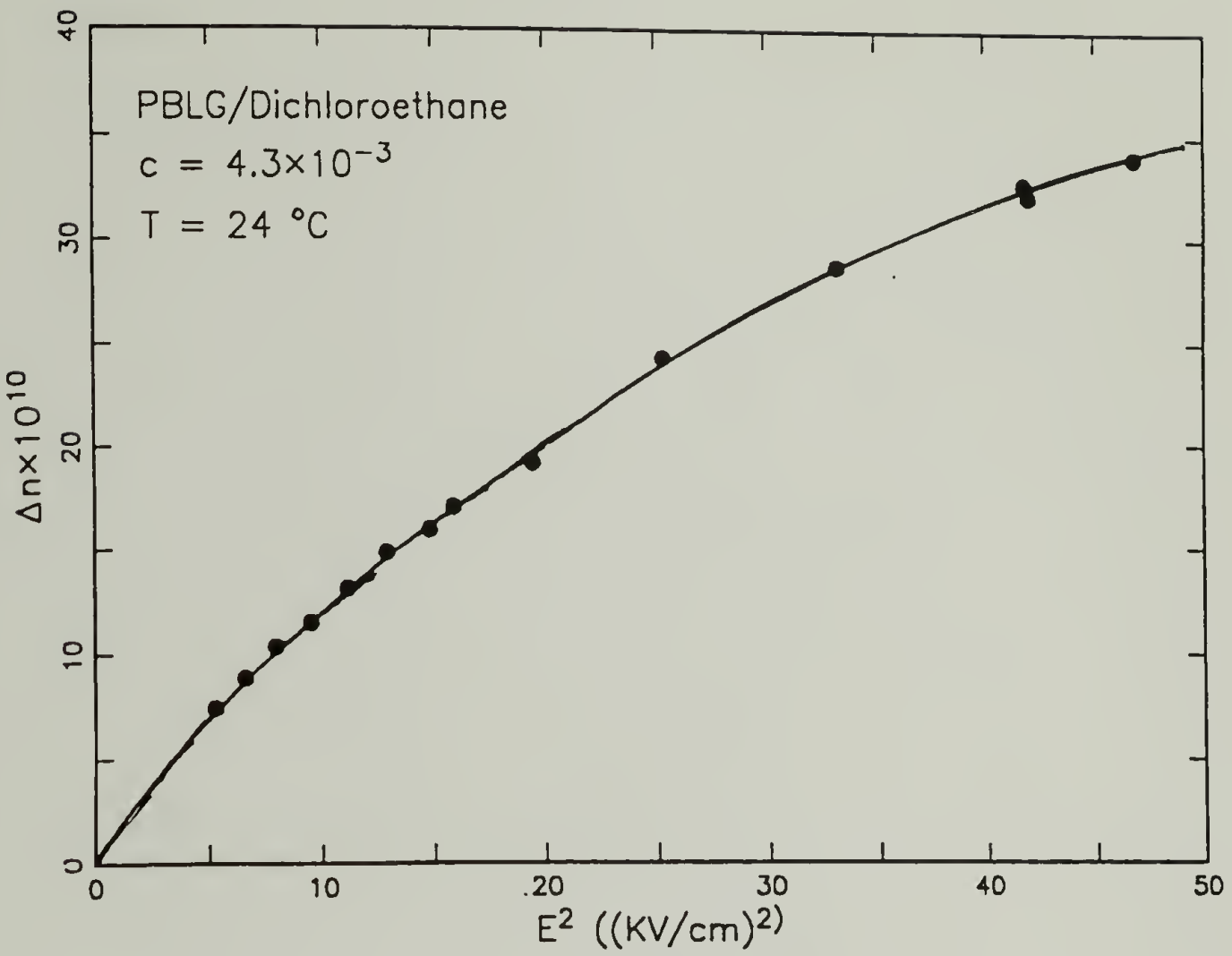

Figure 13 Electric birefringence as a function of square of the electric field for very dilute solution of PBLG in dichloroethane ($c = 4.3 \times 10^{-3}$) at 24 °C.

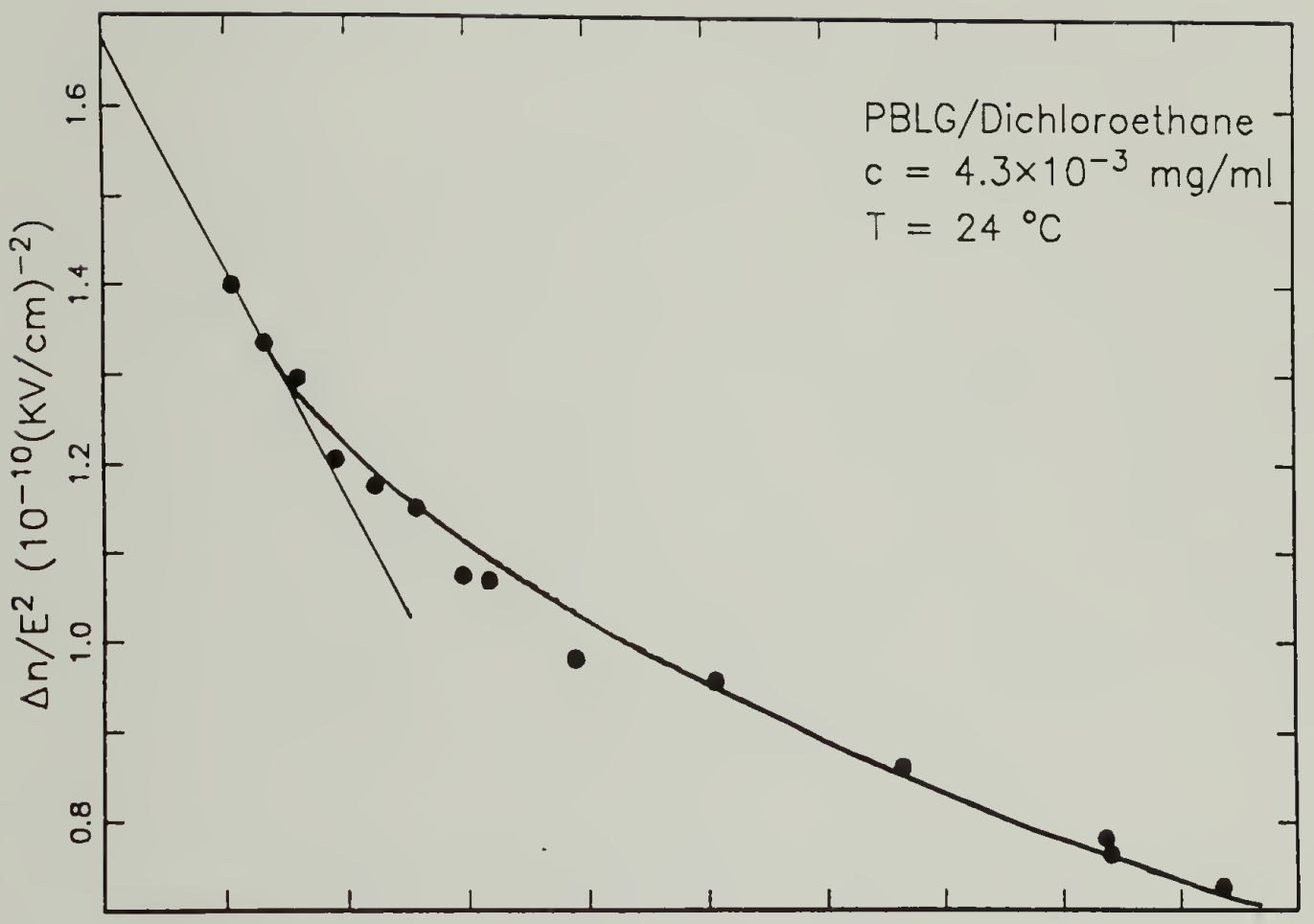

Figure 14 Plot of $\Delta n/E^2$ versus E^2 for PBLG in dichloroethane at 24 °C.

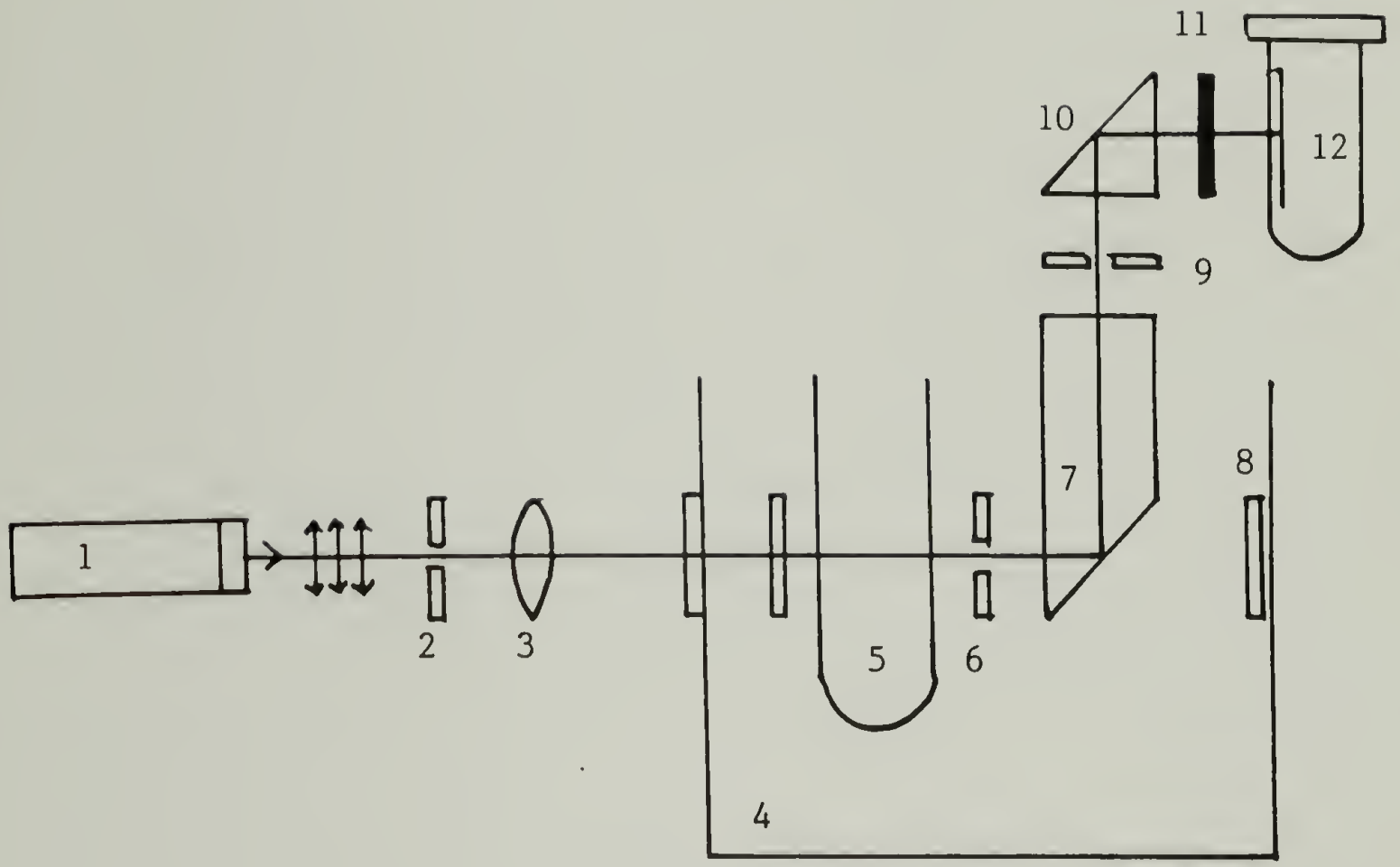

Figure 15 Schematic diagram of the SOFICA light scattering instrument. Components 1-12 are explained in the text.

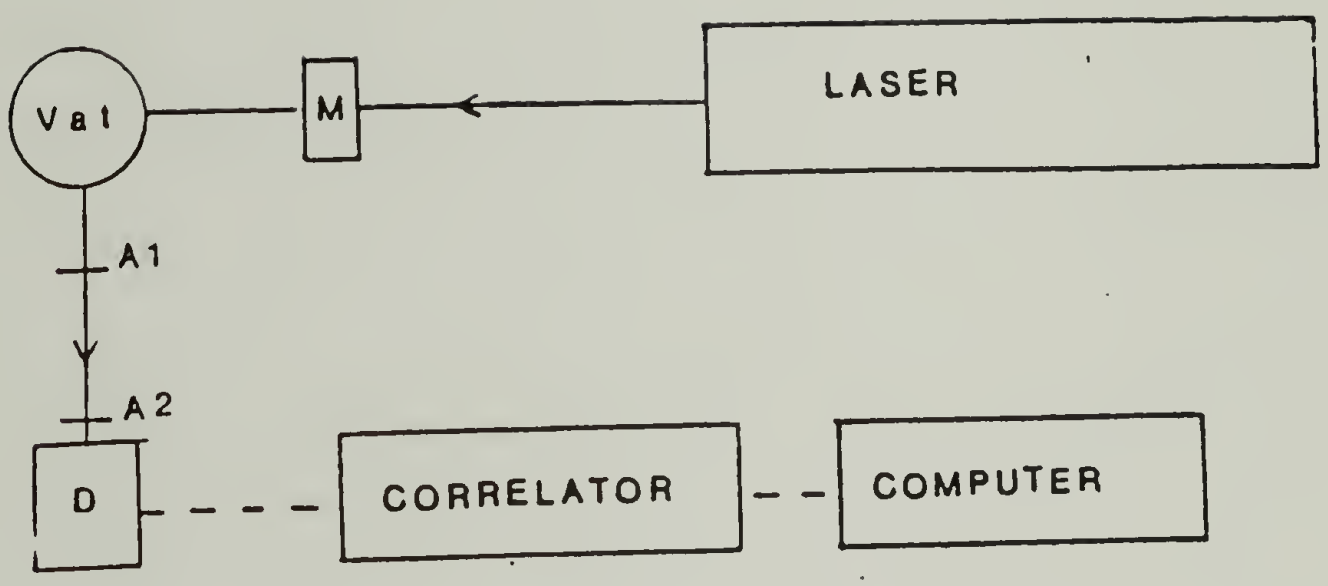

Figure 16 Schematic diagram of the instrument used for depolarized light scattering. M - Monitor D - Detecter A - Aperture

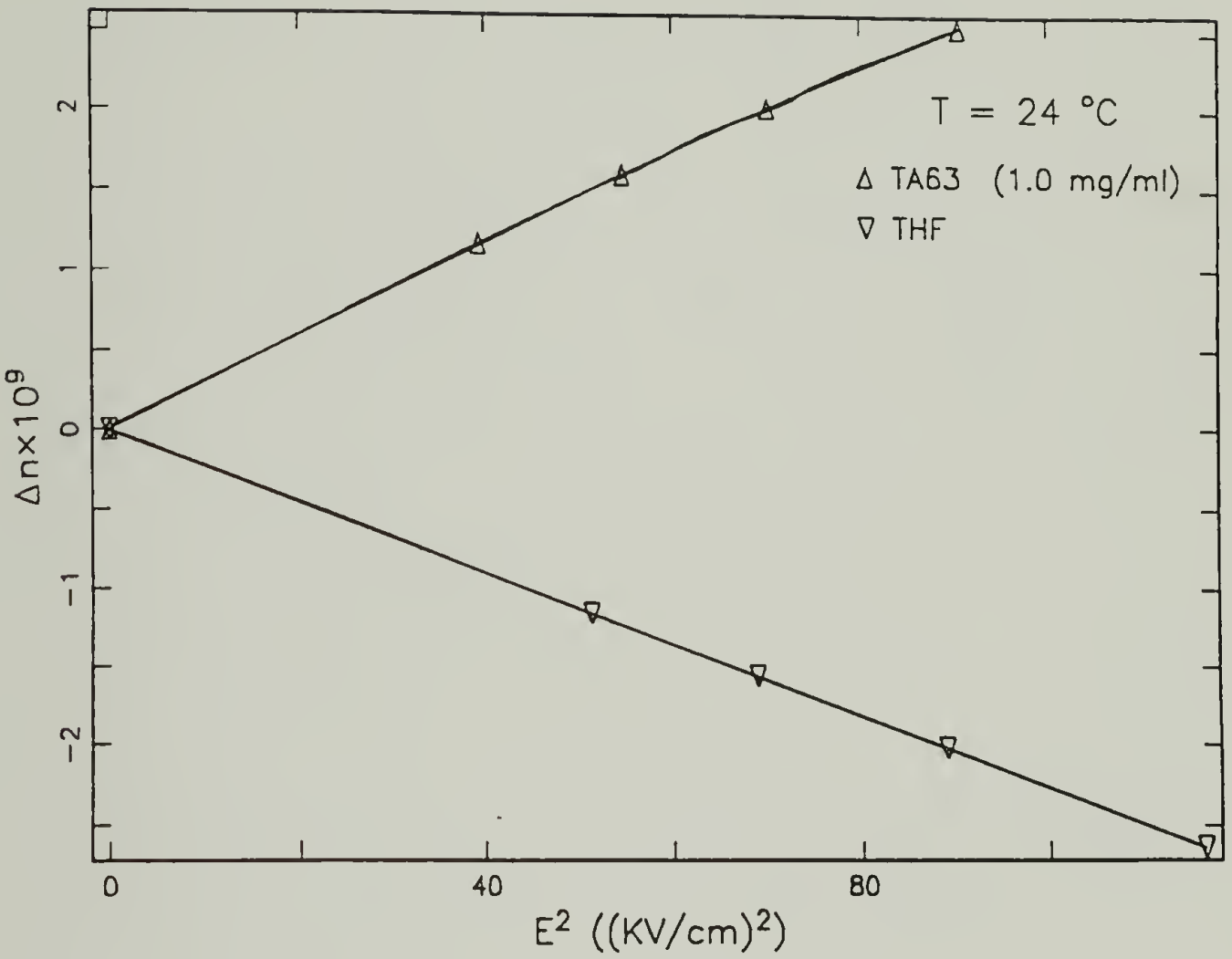

Figure 17 Kerr law for THF and TA63 in THF (1.0 mg/ml) at 24 °C.

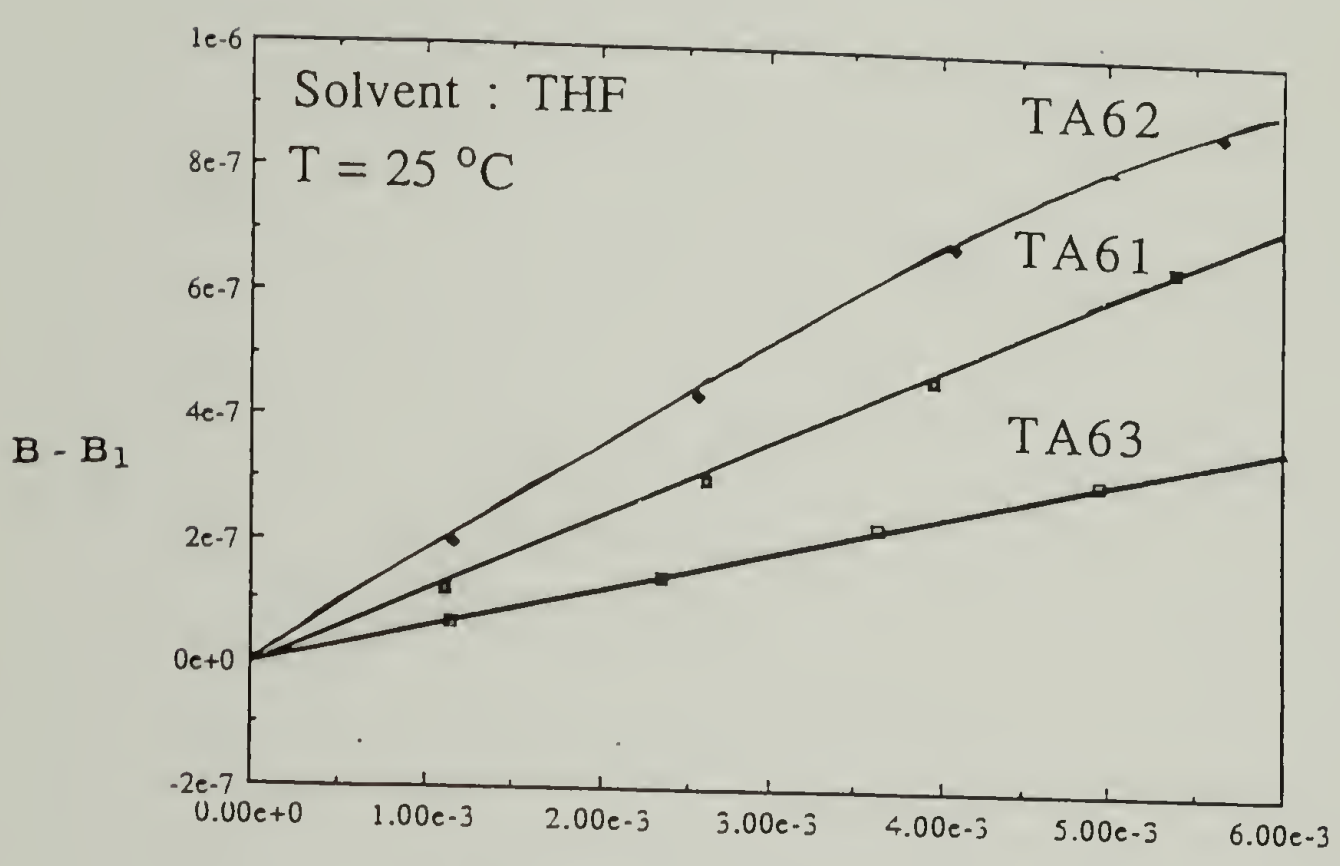

Figure 18 Excess Kerr constant due to samples TA61, TA62 and TA63 in THF at 25 °C as a function of polymer weight fraction.

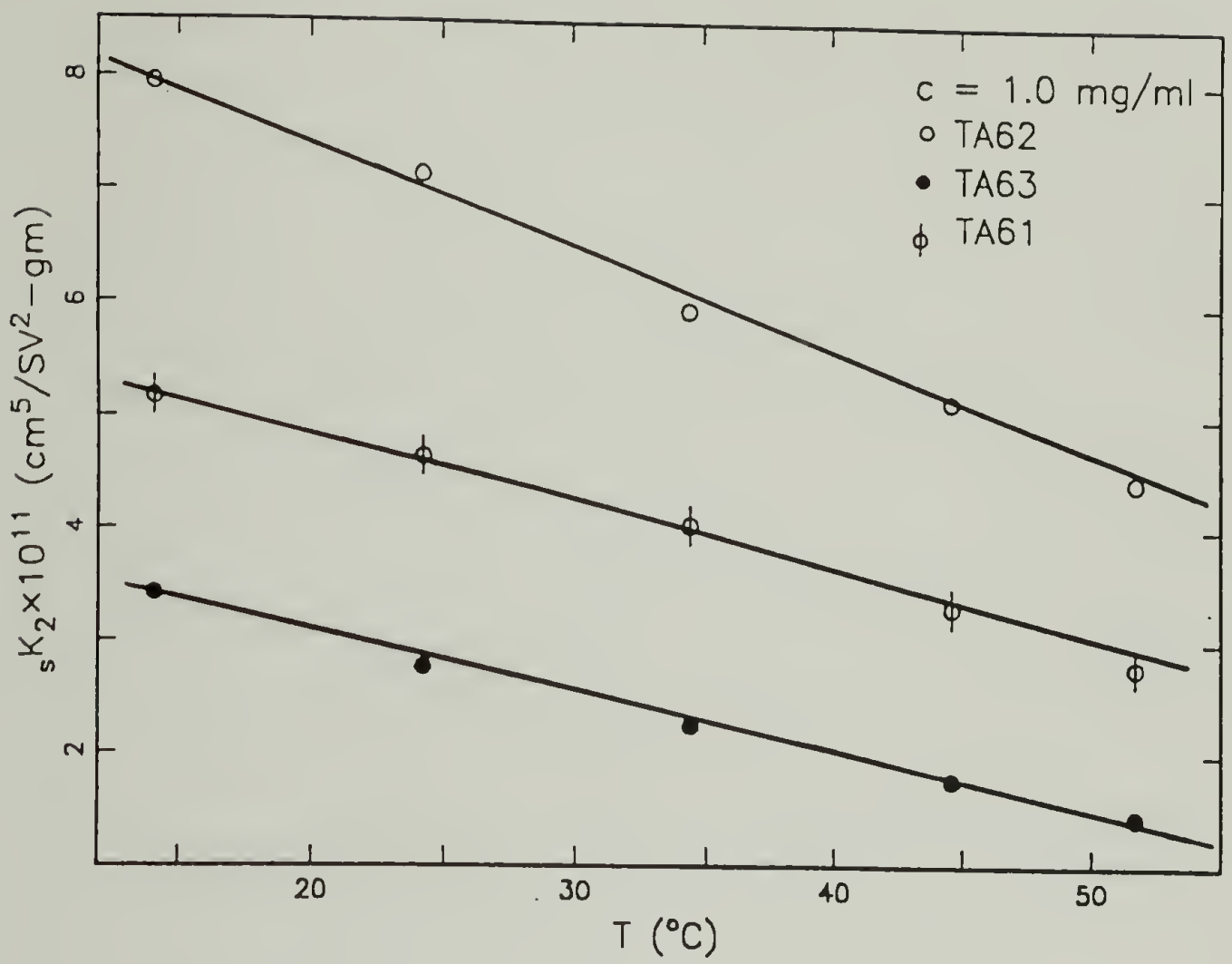

Figure 19 Temperature dependence of the specific Kerr constant, $_sk_2$ for samples TA61, TA62 and TA63.

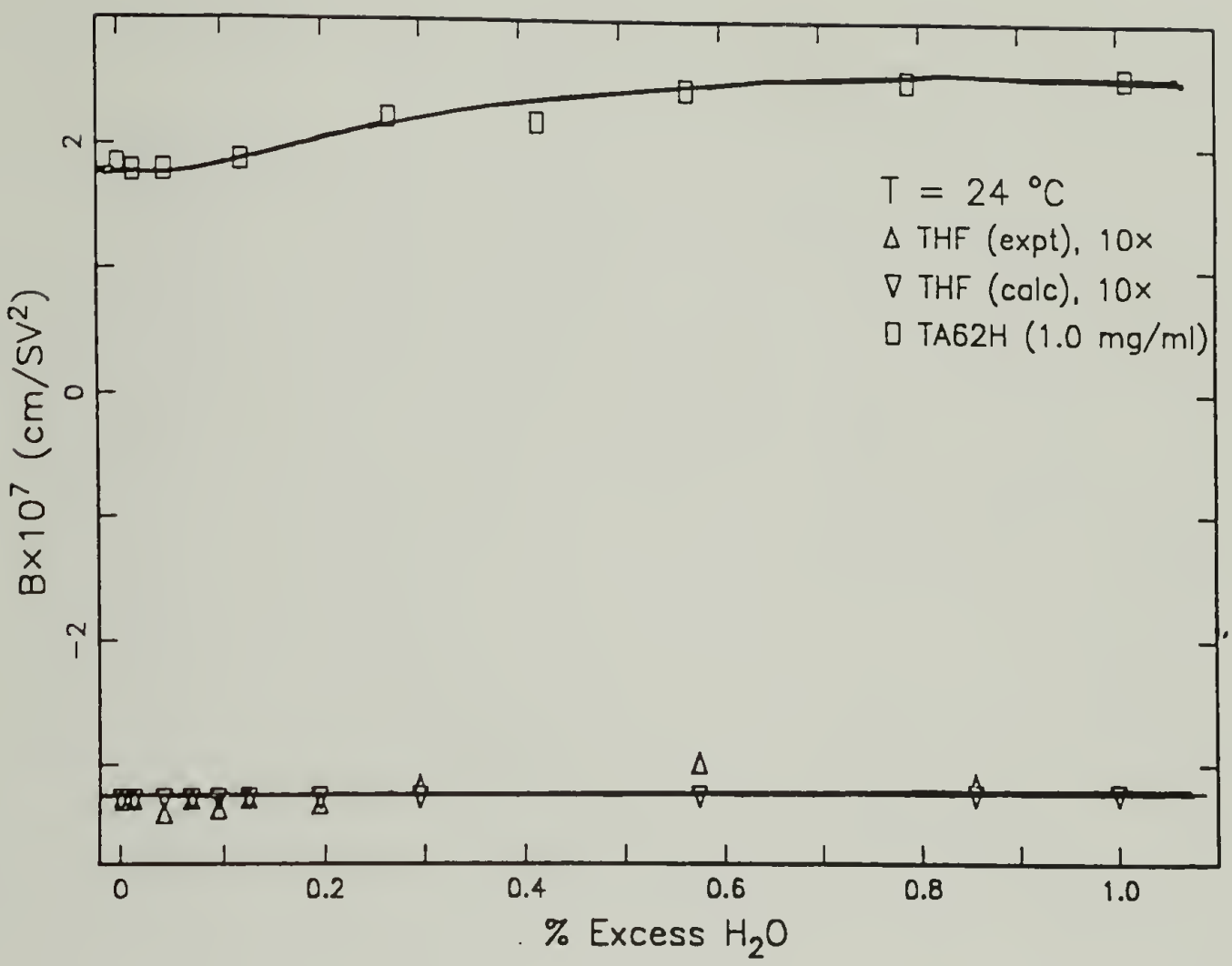

Figure 20 Kerr constant as a function of percent excess water added for THF and TA62 in THF.

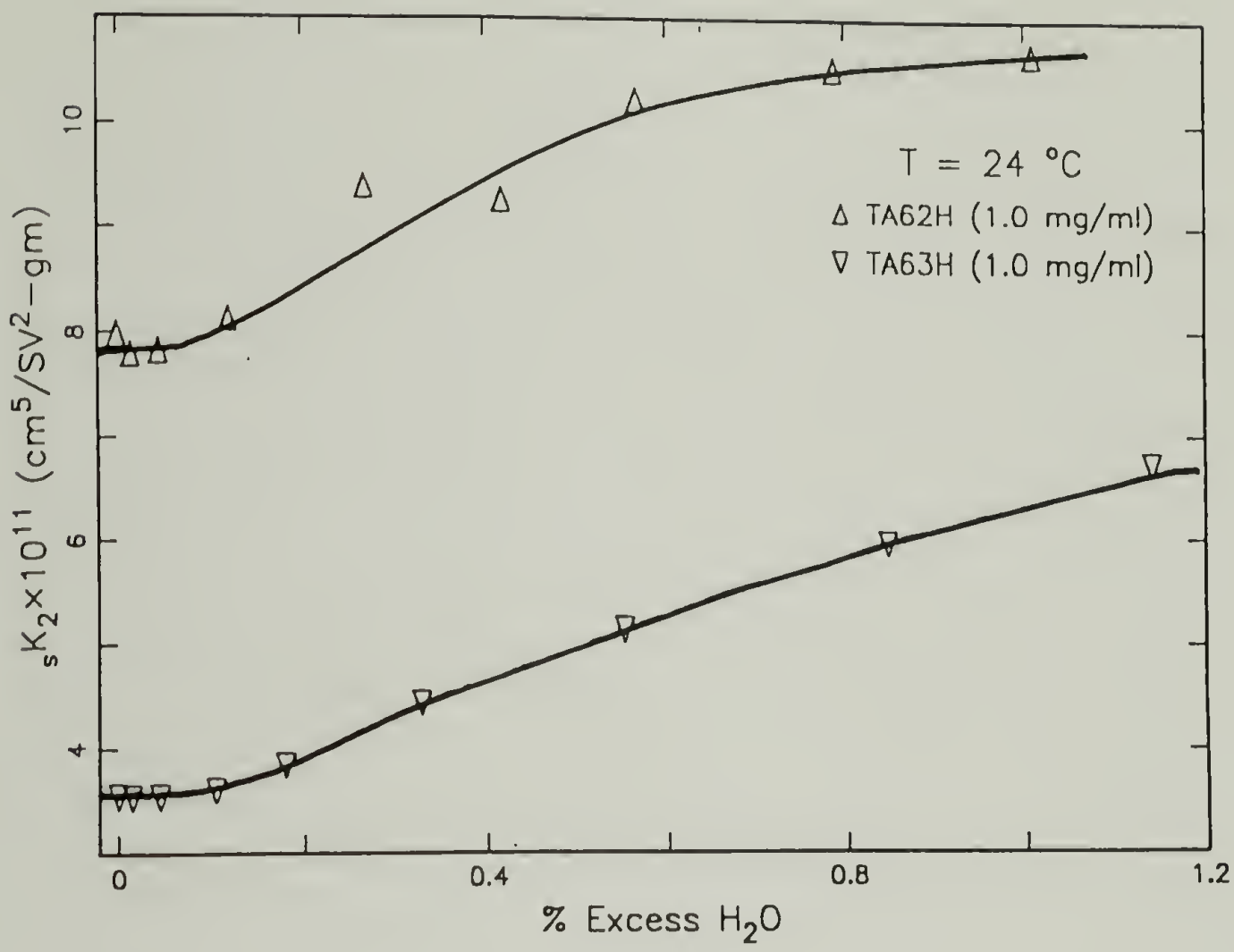

Figure 21 Kerr constant as a function of percent excess water added to TA62 and TA63 in THF.

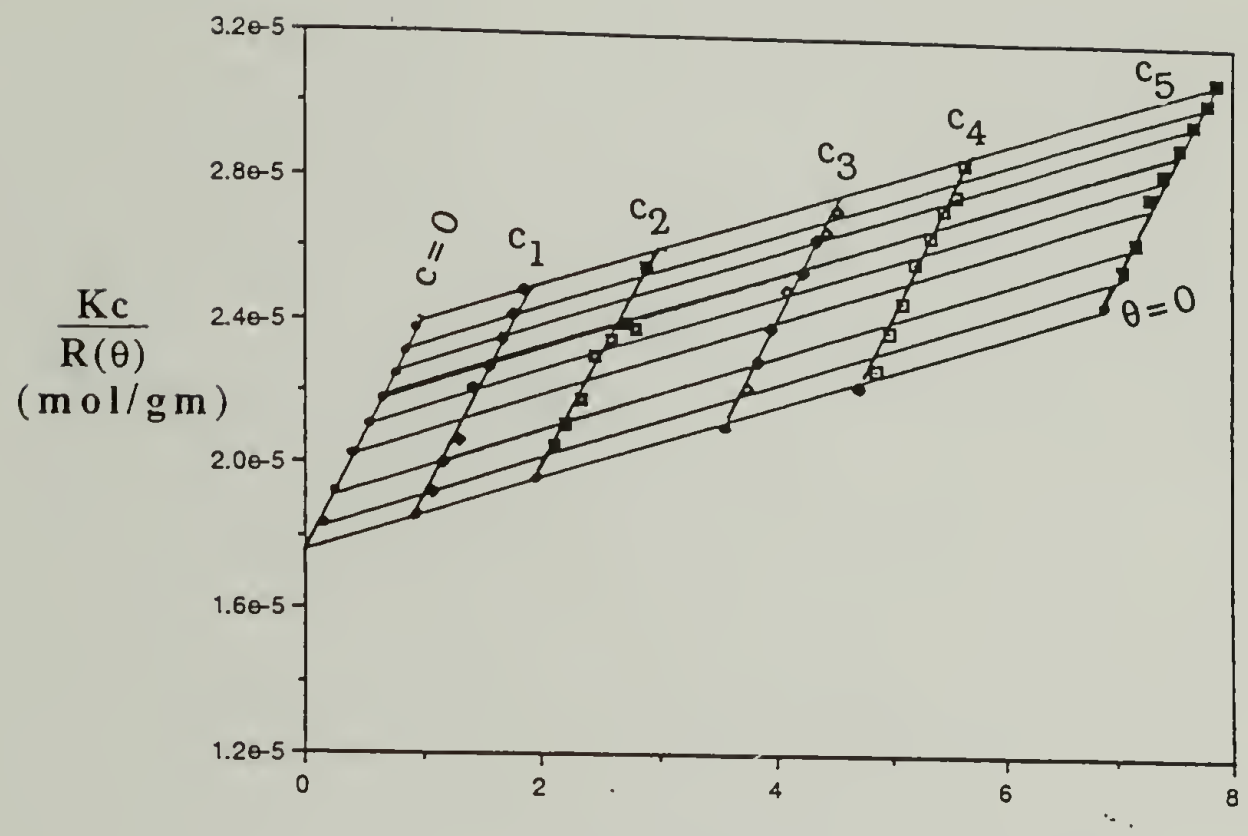

Figure 22 Zimm plot of elastic light scattering from solutions of samples TA63 in THF at 25 °C obtained with the SOFICA light scattering instrument.

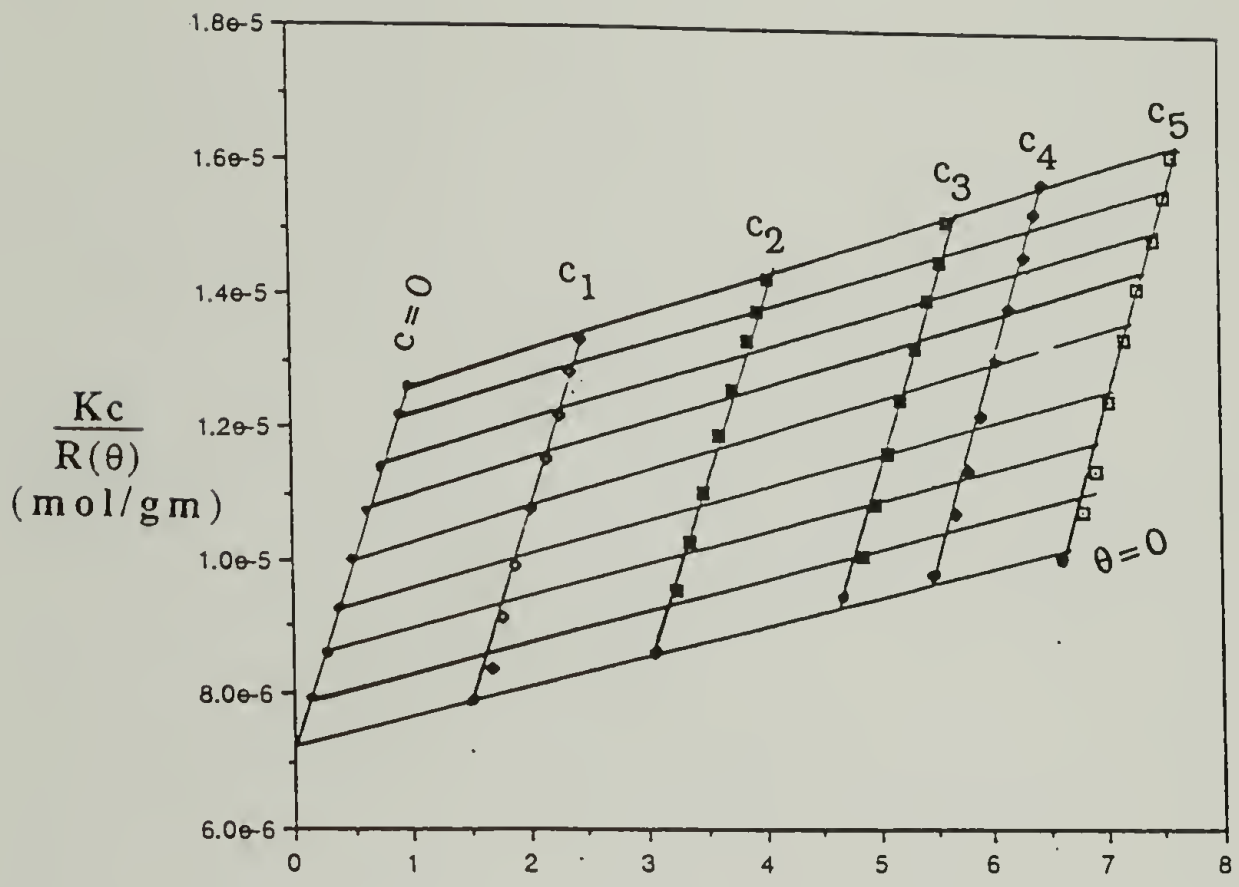

Figure 23 Zimm plot of elastic light scattering from solutions of samples TA61 in THF at 25 °C obtained with the SOFICA light scattering instrument.

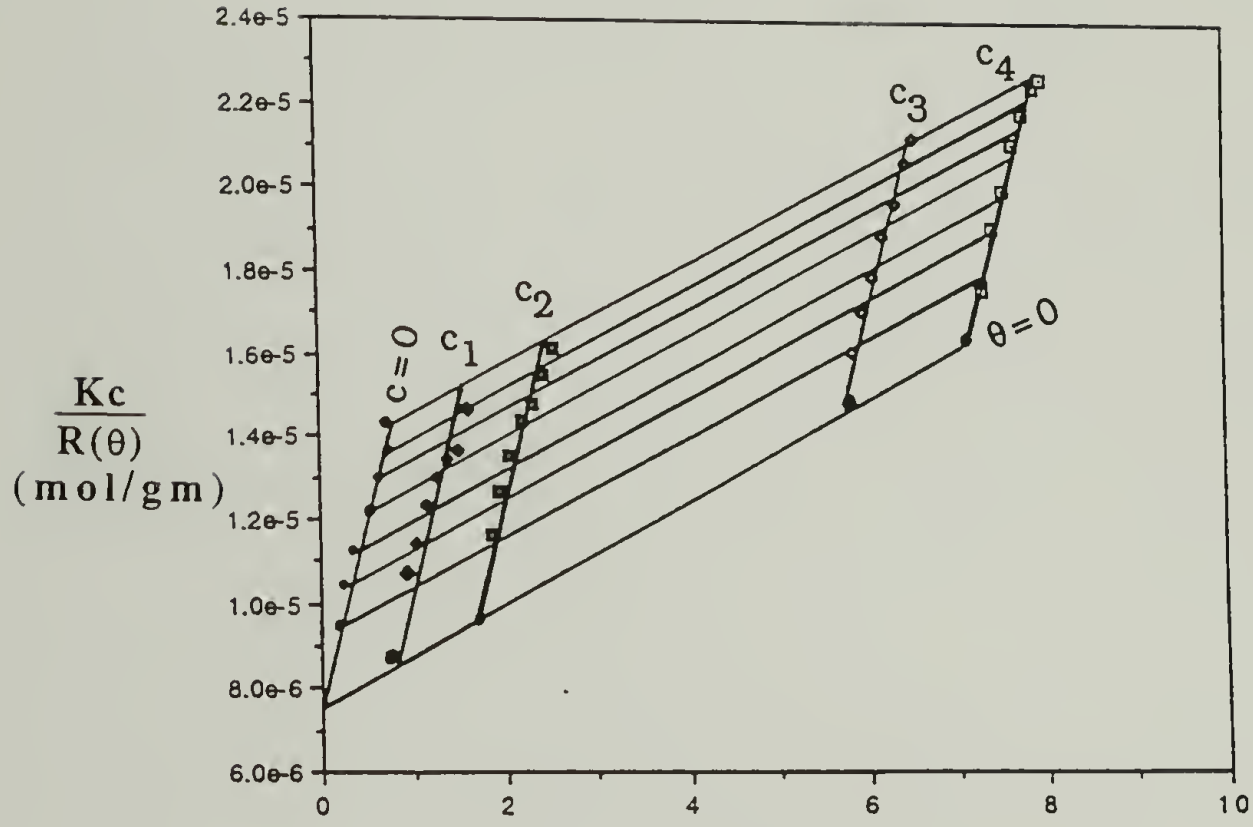

Figure 24 Zimm plot of elastic light scattering from solutions of samples TA62 in THF at 25 °C obtained with the SOFICA light scattering instrument.

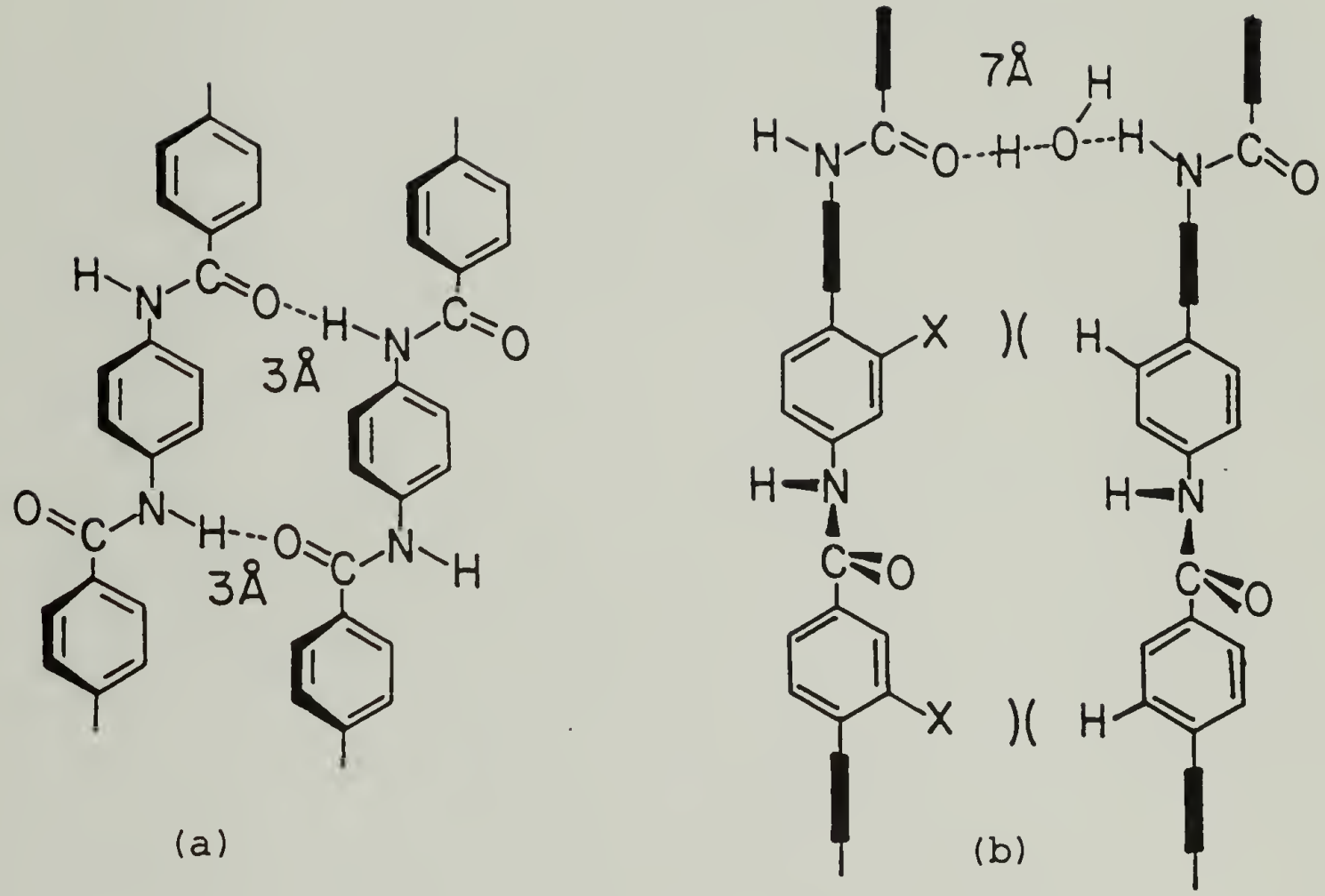

Figure 25 Hydrogen bonding in p-aromatic polyamides. (a) Single phenyl ring allowing close packing (b) substituted biphenyls preventing close packing.

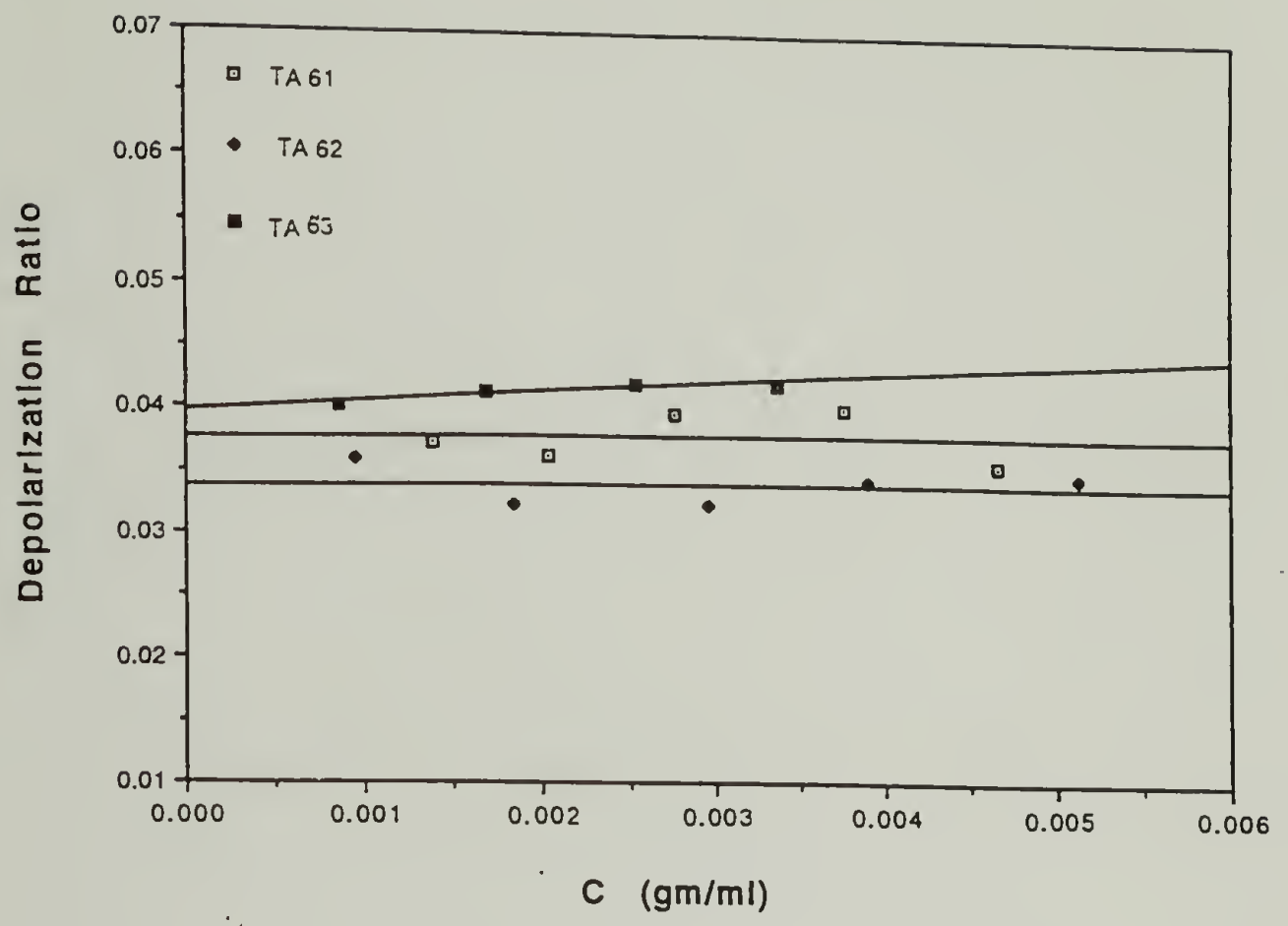

Figure 26 Depolarization ratio at 515 nm as a function of concentration for samples TA61, TA62 and TA63 in THF at 25 °C.

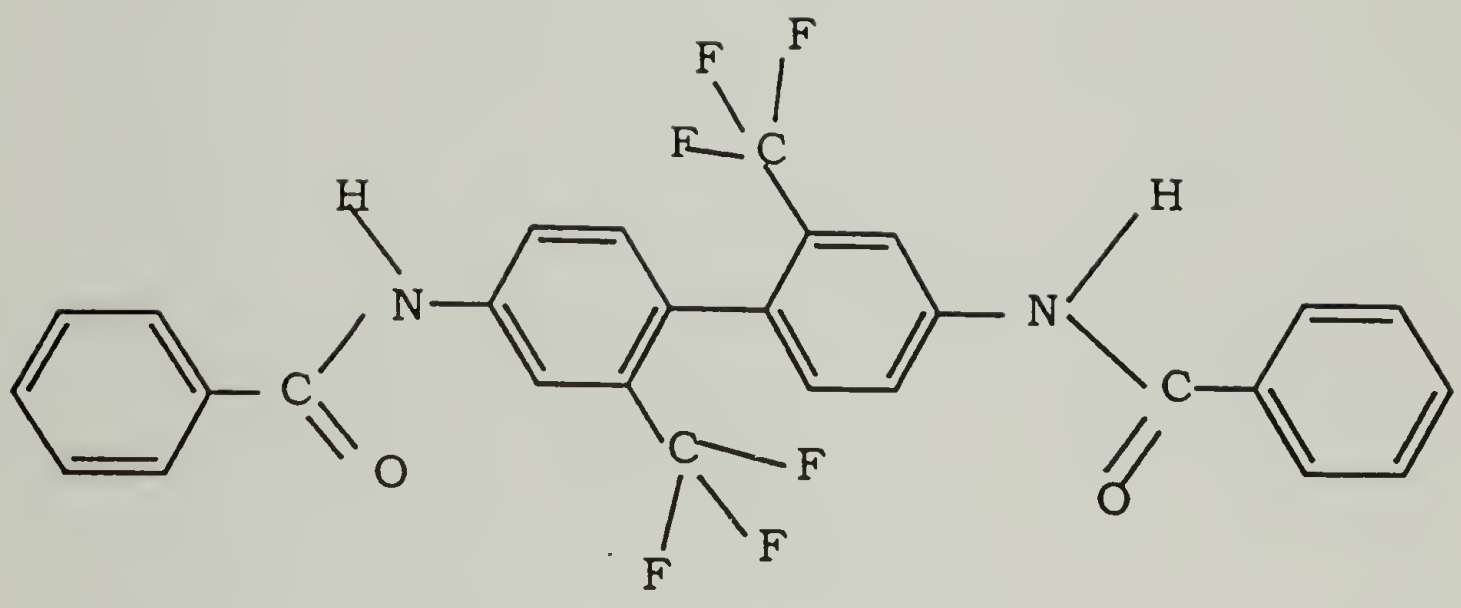

Figure 27 Chemical structure of the compound used to model the repeat unit of the polyamide studied.

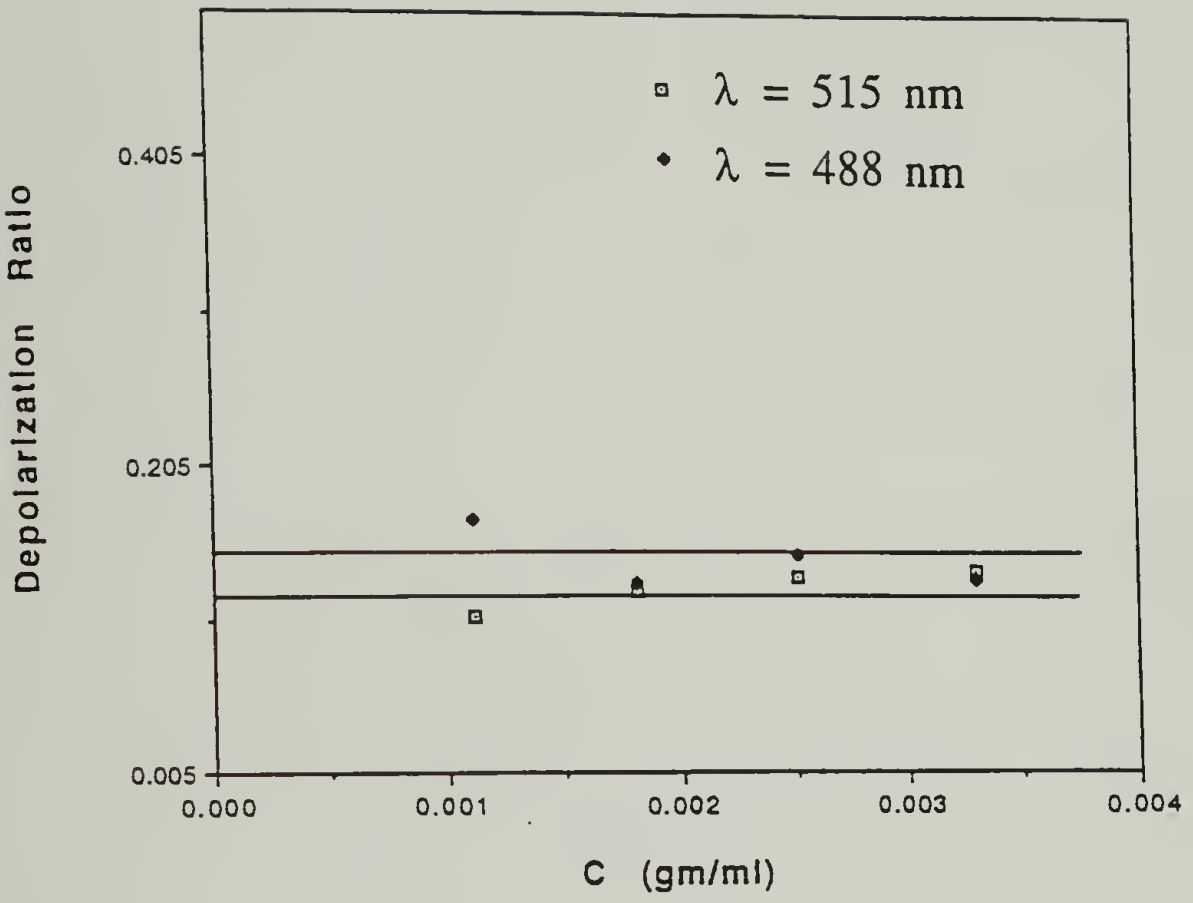

Figure 28 Depolarization ratio at 515 and 488 nm as a function of concentration for the model compound in THF at 25 °C.

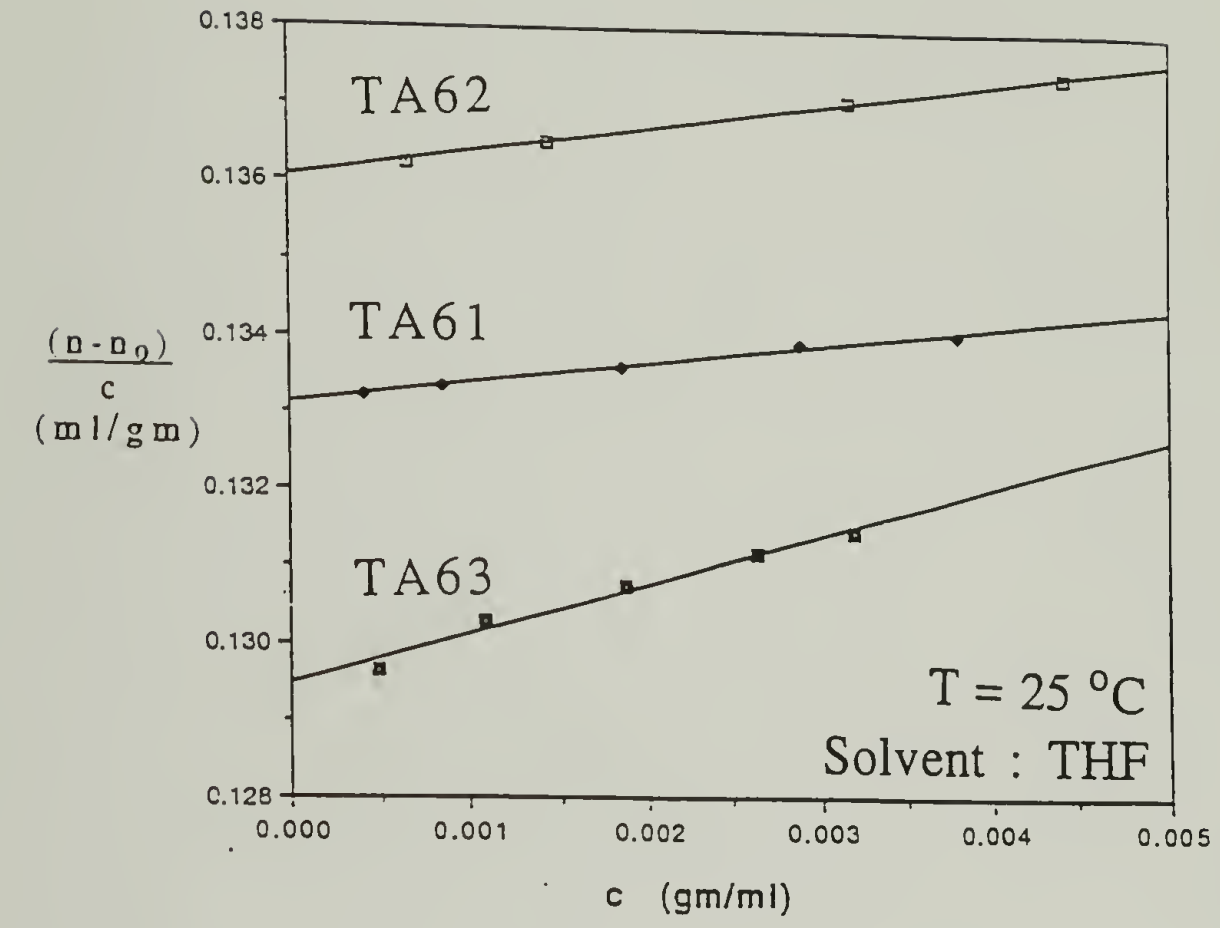

Figure 29 Plot to evaluate dn/dc for samples TA61, TA62 and TA 63 in THF at 25 °C, by extrapolation to zero concentration.

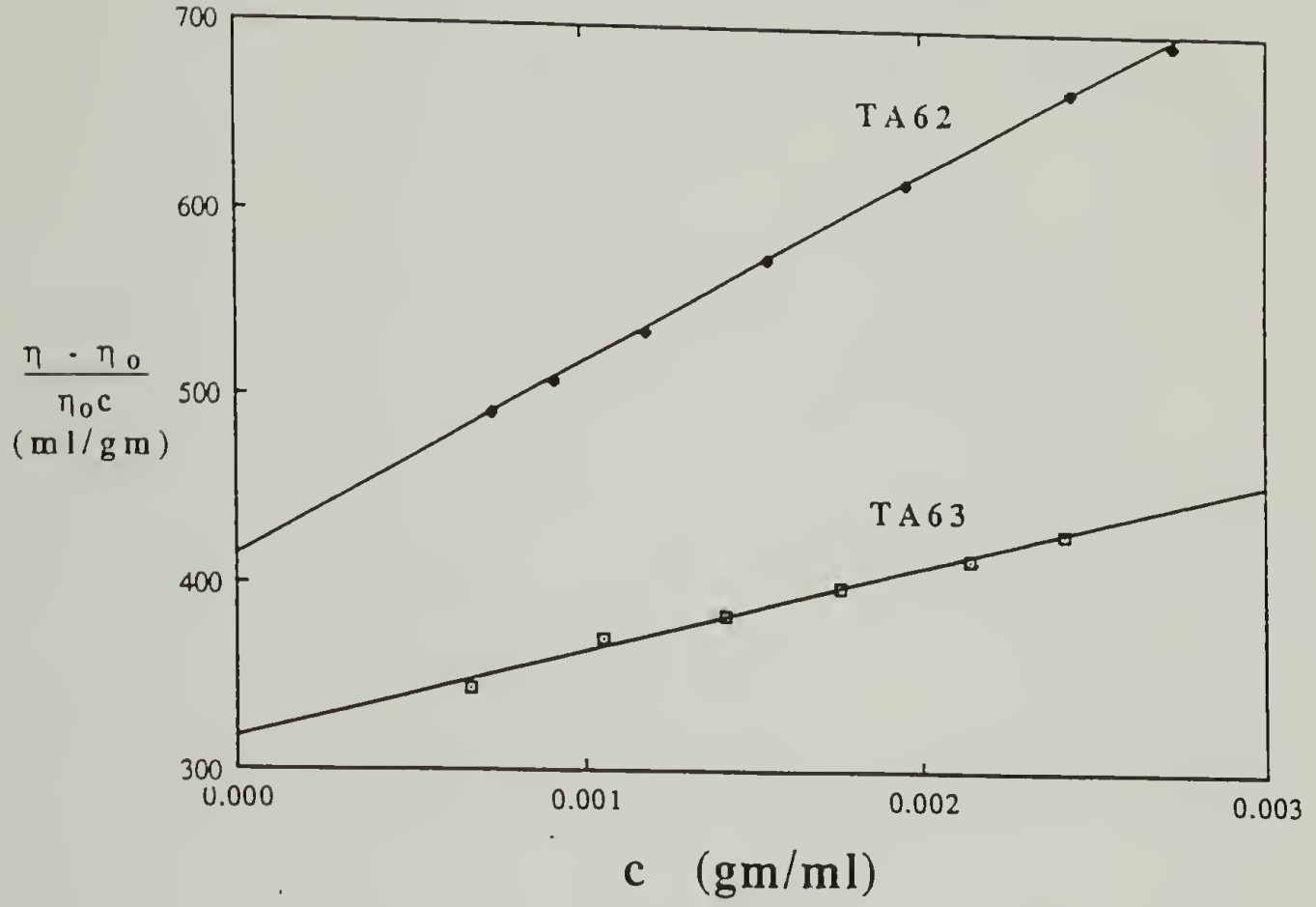

Figure 30 Reduced viscosity η_{sp}/c as a function of concentration for samples TA62 and TA63 in THF at 31 °C.

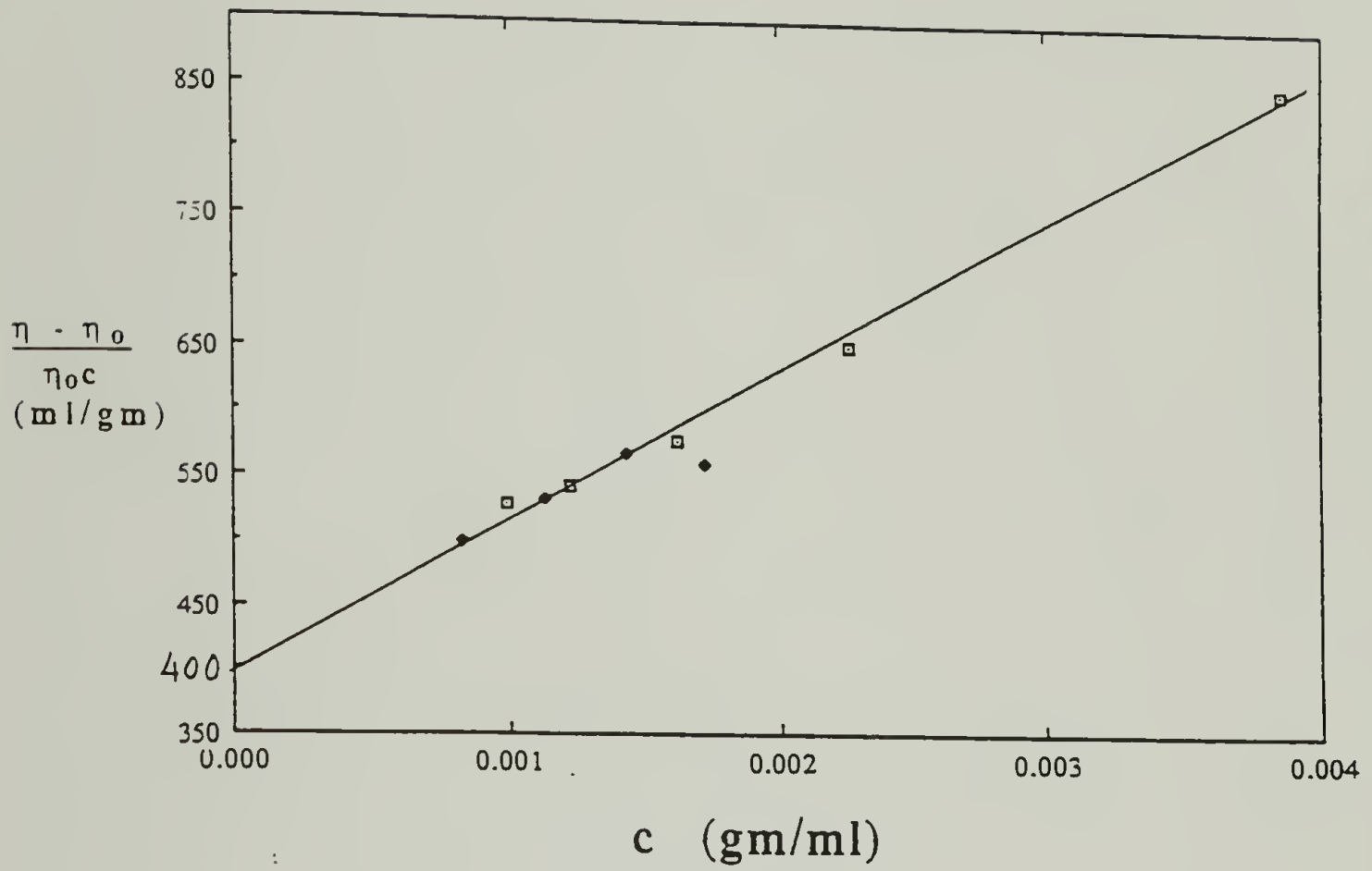

Figure 31 Reduced viscosity η_{sp}/c as a function of concentration for sample TA61 in THF at 31 °C for two different runs.

APPENDIX

HIGH VOLTAGE POWER SUPPLY

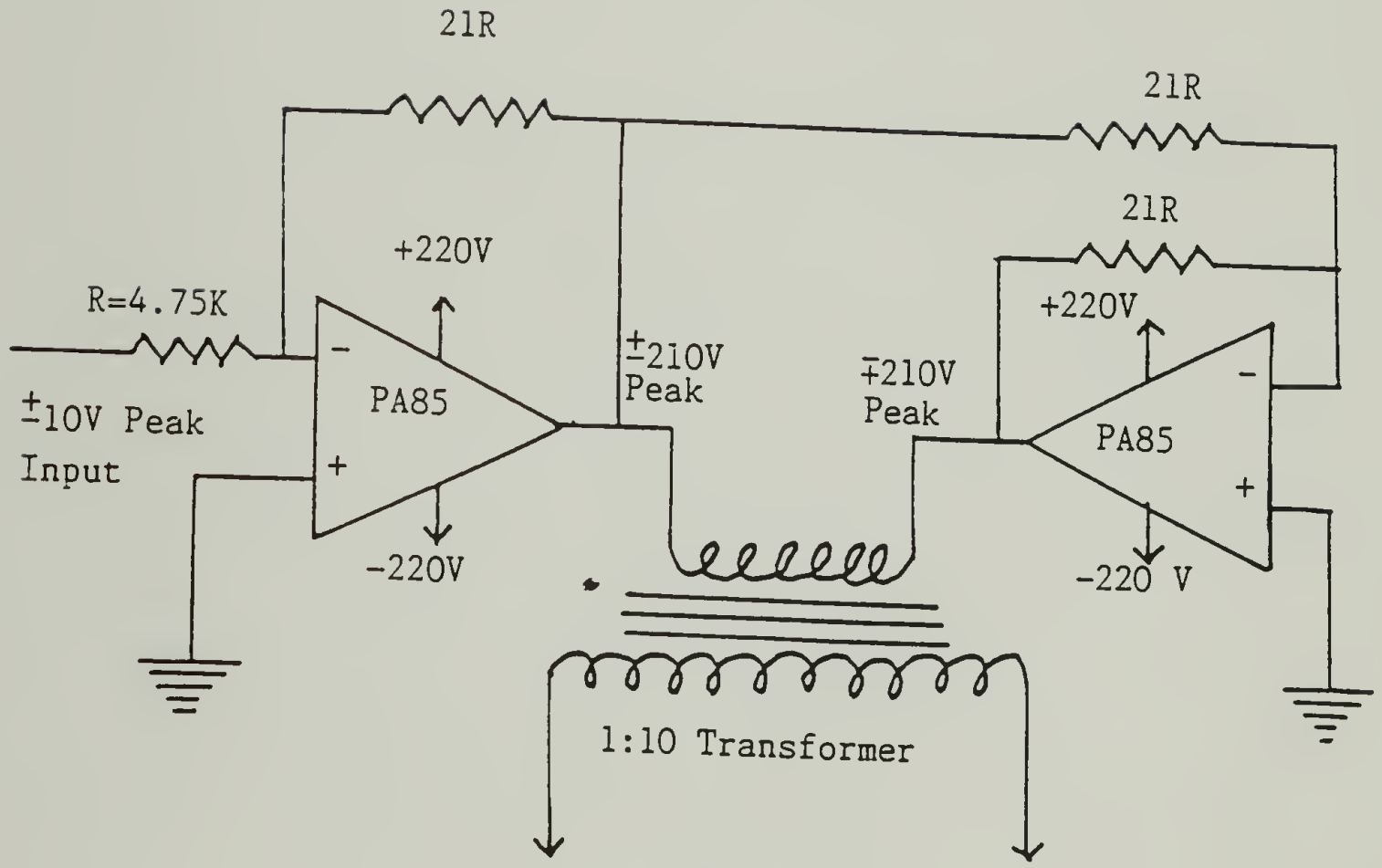

Output
± 4.2 kV Peak

REFRENCES

1. Khanarian, G. and Tonelli, A. E., *J. Chem. Phys.*, **75**, 5031 (1981).

2. Lefevre, C. G. and LeFevre, R. J. W., *Techniques of Chemistry*, Editor: Weissberger, A., Wiley-Interscience, New York, **I**, Pt IIIc, Chap 6 (1972).

3. Flory, P. J., Saiz, E., and et al., *J. Phys. Chem.*, **85**, 3215 (1981).

4. Burnham, A. K., Buxton, L. W. and Flygare, W. H., *J. Chem. Phys.*, **67**, 4990 (1977).

5. Lezov, A. V., Tsvetkov, N. V. and Trusov, A. A., *Polymer Science U.S.S.R.*, **32**, 1801 (1990).

6. Tsvetkov, V. N., *Rigid Chain Polymers*, Translated by Korolyova, E. A., Consultants Bureau, NY, Chap 7 (1989)

7. Ebert, M., Jungbauer, D. A., Kleppinger, R., Wendorff, J. H. and et al., *Liquid Crystals*, **4**, 53 (1989).

8. Jungbauer, D. A. and Wendorff, J. H., *Mackromol. Chem.*, **189**, 1345 (1988).

9. Kwolok, S. L., U.S. Patent 3 671 542 (1972).

10. Morgan, P., U.S. Patent 3 801 528 (1974).

11. Blades, H., U.S. Patent 3 869 429 (1975).

12. Rogers, H. G. and et al., *Macromolecules*, **18**, 1058, (1985).

13. Gaudiana. R. A., Minns, R. A. and et al., *Prog. Polym. Sci.*, **14**, 47 (1989).

14. Trefonas III, P., Djurovich, P. I., Zhang, X. M., West, R., Miller, R. D., Hofer, D., *J. Poly. Sci., Poly. Lett. Ed.*, **21**, 819 (1983).

15. Trujilla, R. E., *J. Organomet. Chem.*, **198**, 27 (1980).

16. Pitt, C. G., *Homoatomic Rings, Chains and Macromolecules of the Main Group Elements*, Editor: Rheingold, A. L., Elsevier, NY (1977).

17. Trefonas III, P., Damewood, J. R. Jr., West, R., Miller, R. D., *Organometallics*, **4**, 1318 (1985).

18. Harrah, L. A., Ziegler, J. M., *J. Polymer Science Poly. Lett. Ed.*, **23**, 209 (1985).

19. Cotts, P. M., *Proceedings of Polymer Materials*, Science and Engineering Division : Washington, D.C., **53**, 336 (1985).

20. Flory, P. J., *Principles of Polymer Chemistry*, Cornell University Press, Ithaca, New York (1953).

21. Horn, P., *Ann. Phys.*, **10**, 386 (1955).

22. Utiyama, H. and Kurata, M., *Bull. Inst. Chem. Res. Kyoto Univ.*, **42**, 128 (1964).

23. Benoit, H., C. R. *Acad. Sci.*, **236**, 687 (1953).

24. Benoit, H. and Doty, P., *J. Phys. Chem.*, **57**, 958 (1953).

25. Kuhn, W., *Kolloid Z.*, **76**, 258 (1939).

26. Yamakawa, H., *Modern Theory of Polymer Solutions*, Harper and Row, New York, Chap 2 (1971).

27. Nagai, K., *Polymer Journal*, **3**, 67 (1972).

28. Hummel, J. P. and Flory, P. J., *Macromolecules*, **13**, 479 (1980).

29. Erman, B., Flory, P. J. and Hummel, J. P., *Macromolecules*, **13**, 484 (1980).

30. Flory, P. J., *Chem. Rev.*, **39**, 137 (1946).

31. Flory, P. J., *High Molecular Weight Organic Compounds (Frontiers in Chemistry)*, Editors: Burk, R. E. and Grummitt, O., Interscience, New York, Vol 6 (1949).

32. Kerr, J., *Phil. Mag.*, **50(4)**, 337, 446 (1875).

33. Beams, J. W., *Reviews of Modern Physics*, **4**, 133 (1932).

34. Le Fevre, C. G. and Le Fevre, R. J. W., *J. Chem. Soc.*, 4041 (1953).

35. Buckingham, A. D. and Pople, J. A., *Proc. Phys. Soc. London*, Sect. **A68**, 905 (1955).

36. Kerker, M., *The Scattering of Light and other Electromagnetic Radiation*, Academic Press, New York (1969).

37. Van de Hulst, H. C., *Light Scattering by Small Particles*, John Wiley and Sons, New York (1957).

38. Einstein, A., *Ann. de Physik*, **33**, 1275 (1910).

39. Huglin, M. B., *Light Scattering from Polymer Solutions*, Academic Press, London (1972).

40. Huglin, M. B. and Sokro, M. B., *Polymer*, **21**, 651 (1980).

41. Zimm, B. H., *J. Chem. Phys*, **16**, 1093 (1948).

42. Zimm, B. H., *J. Chem. Phys.*, **16**, 157 (1948).

43. Utiyama, H., *J. Phys. Chem.*, **69**, 4138 (1965).

44. Utiyama, H. and Kurata, M., *Bull. Inst. Chem. Res. Kyoto Univ.*, **42**, 128 (1964).

45. Kirkwood, J. G. and Riseman, J., *J. Chem. Phys.*, **16**, 565 (1948).

46. Auer, P. L. and Gardner, C. S., *J. Chem. Phys.*, **23**, 1545 (1955); **23**, 1546 (1955).

47. Muthukumar, M., *J. Chem. Phys.*, **81**, Pt II, 6272 (1984).

48. Hatziavramidis, D. and Muthukumar, M., *J. Chem. Phys.*, **83(5)**, 2522 (1985).

49. Riseman, J. and Kirkwood, J. G., *J. Chem. Phys.*, **18**, 512 (1950).

50. Kirkwood, J. G. and Auer, P. L., *J. Chem. Phys.*, **19**, 281 (1951).

51. Yamakawa, H. and Fujii, M., *Macromolecules*, **7**, 128 (1974).

52. Kratky, O. and et al., *J. Poly. Sci.*, Pt C, **31**, 311 (1970).

53. LeFevre, C. G. and LeFevre, R. J. W., *Rev. Pure Appl. Chem.*, **5**, 261 (1955).

54. Boyle, L. L., Buckingham, A. D., Disch, R. L. and Dunmer, D. A., *J. Chem. Phys.*, **45**, 1318 (1965).

55. *International Critical Tables*, **VII**, McGraw Hill, New York (1930).

56. O'Konski et al., *J. Phys. Chem.*, **63**, 1558 (1959).

57. Chu, B., Wu, D. Q. and Wu, C., *Rev. Sci. Instrum.*, **58**, 1158 (1987).

58. Shablygin, M. V., Nikitina, O. A., Belousova, T. A. and Kudryavtsev, G. I., *Vysokomol. Soedin.*, Ser A, **24**, 984 (1982).

59. Brandrup, J. and Immergut, E. H. (Editors), *Polymer Handbook*, John Wiley & sons, New York (1975).

60. Flory, P. J., *Proc. Roy. Soc. London.*, Ser A, **234**, 73 (1956).

61. Onsager, L., *Ann. N. Y. Acad. Sci.*, **51**, 627 (1949).

62. Ishihara, A., *J. Chem. Phys.*, **18**, 1446 (1950); **19**, 1142 (1951).

63. Odijk, T., *Macromolecules*, **19**, 2313 (1986).